Stony Brook University

Investigation of Biomineralization by Raman Spectroscopy

A Thesis Presented

by

Robert William Fatscher

to

The Graduate School

in Partial Fulfillment of the

Requirements

for the degree of

Master of Science

in

Materials Science and Engineering

Stony Brook University

August 2014

Stony Brook University

The Graduate School

Robert William Fatscher

We, the thesis committee for the above candidate for the

Master of Science degree, hereby recommend

acceptance of this thesis.

Molly Gentleman – Thesis Advisor
Assistant Professor, Department of Materials Science and Engineering

Miriam Rafailovich
Dist. Professor, Department of Materials Science and Engineering

Yizhi Meng
Assistant Professor, Department of Materials Science and Engineering

This thesis is accepted by the Graduate School

Charles Taber
Dean of the Graduate School

Abstract of the Thesis

Investigation of Biomineralization by Raman Spectroscopy

by

Robert William Fatscher

Master of Science

in

Materials Science and Engineering

Stony Brook University

2014

Abstract

Biomineralization is a process in which living organism grow composite materials consisting of inorganic and organic materials. This produces a composite material consisting of both inorganic and organic components, with superior mechanical properties. In the human body bone and dentin are both examples of biominerals. In this research Raman spectroscopy was used to characterize dentin from mice and human teeth, to determine composition. In the mouse tooth samples areas of irregular dentin were found, along the inside of the tooth, to be in the process of mineralization. By analyzing the samples along these areas we were able to determine the composition of dentin and track how it changed in these area. By analysis of the mineral to matrix ratio the areas of irregular dentin were determined to have less mineral present. Observations of other organic components and collagen in increased concentrations in this area suggested these area were in the process of biomineralization.

The understanding of the structure of dentin and it's biomineralization process is of crucial importance when trying reproduce dentin. Scientists and engineers are able to produce

dentin minerals *in vitro* by culturing various dental stem cells. The ability to create dentin mineral from cells could lead to methods of repairing dentin in patients, or even lead to the creation of a completely engineered tooth. While dentin-like materials can be produced in a laboratory environment, analysis and comparison of the composition of these materials must be performed to ensure the mineral produced is consistent with dentin. Mineralized nodules from six different dental stem cell lines were cultured to produce a mineralized deposit. Utilizing Raman spectroscopy, we were able to determine cell source dependent differences in a variety of dental stem cells, and compare the mineral produced to native dentin.

Orthopedic implants are implants used to replace damaged bone, examples include knee, hip and dental implants. These implants are designed to osteointegrate with the native healthy tissues in order to create a functionally stable and structural interface. Biomaterials such as hydroxyapatite and titania are known to increase the rate of bone regeneration *in vivo*.[1] By accelerating the early response of bone forming cells to these implants, better fixation is achieved between the implant and the bone, shortening recovery times and increasing the viability of these implants. In the last part of this research an investigation of osteoblasts cultured at 14 days on five different heat-treated titania substrates was investigated by Raman spectroscopy, in order to observe the initial cellular response to the titania substrates. The heat-treatment of titania changes the amount of oxygen on it's surface which in turn effects the surface energy. A change in the surface energy of a material will affect the cellular response, by culturing cells on various heat-treated titania substrates a relationship between the surface energy and cellular response can be investigated. A faster cellular response would lead to an increased rate of bone regeneration shortening healing times and allowing for better fixation of the implant.

Dedicated to

My Mother and Father

Table of Contents

List of Figures

List of Tables

Acknowledgements

I would like to thank Dr. Gentleman for her help and support over the course of my research and graduate career, and for helping me with my application for graduate school. I would also like to thank Dr. Rafailovich and Dr. Meng for serving on my committee.

I would also like to thank everyone in our group past and present, especially Priya Dadd for her help with my experiments.

1.0 - Introduction

1.1 - Biological Apatites

Biominerals are composite materials consisting of organic and inorganic components, made by living organisms. Biominerals are found in a wide variety of forms across many different species, including teeth and bones. Bones and teeth make up the skeletal system and provide a wide range of functions, including support, movement, protection, production of blood cells and storage of minerals. The combination of both inorganic minerals and organic materials in a hierarchal structure, produces material with superior mechanical properties exceeding those of its individual components.[2] Bone and dentin are comprised of an inorganic mineral hydroxyapatite, collagen fibers and organic polymers.[3-5] Formed from a carefully controlled process where a collagen scaffold provides a template for the deposition of the hydroxyapatite mineral, initiated by the other non-collagenous proteins.[6]

Hydroxyapatite has the molecular formula $Ca_{10}(PO_4)_6(OH)_2$, and belongs to the hexagonal crystal system.[7] Various substitutions in the matrix can occur, which alter the crystal structure and mechanical properties. For example, the hydroxyl group can be replaced with a fluoride, chloride or carbonate ion. In natural biominerals the most common substitutions are of carbonate CO_3^{2-}. Two types of CO_3^{2-} substitutions occur, type A and type B. In type A carbonated Hydroxyapatite the OH^- is substituted by with a CO_3^{2-}, causing a vacancy of the other hydroxyl group to compensate the substitution of a monovalent ion by a divalent one.[7] In type B Hydroxyapatite a CO_3^{2-} is in the place of a PO_4^{3-} group creating a calcium and OH^- vacancy.[7] Carbonate substitutions found in hydroxyapatite are predominately type B, leading to a calcium deficient bone mineral. Highly carbonated bone is brittle and less stiff, typical of aged bone.[8,9]

Bone, dentin, and enamel all form in a similar cell-mediated processes. These processes provide the framework for the growth of the hydroxyapatite crystals. Dentin is similar to bone originating from the same class of tissue, the mesoderm. Enamel is formed from the ectoderm a class of tissues responsible for making up the skin.[10,11] Dentin and bone contain about 70% mineral and 30% cells, matrix and proteins. Enamel contains 2-6% protein and 94-98% mineral by weight.[10] The decrease in enamels organic content is due to it maturation. As enamel matures the cells responsible for mineralization die off leaving only 25-30% of the organic component of developing enamel leading to a loss of its regenerative abilities.[11] Bone and dentin mineral is a poorly crystalline calcium deficient apatite, with CO_3^{2-} substitutes for mainly PO_4^{3-}, type B Hydroxyapatite. The average composition of bone and dentin mineral can be described by the molecular formula $Ca_{8.3}(HPO_4, CO_3)_{1.7}(PO_4)_{4.3}(CO_3, OH)_{0.3}$ with $0 \leq x \leq 2$.[12-13] The carbonate containing hydroxyapatite allows for the absorption of proteins. These proteins influence the differentiation of cells to specific classes.[14] While the crystal structure and formation of bone and dentin are very similar, the hierarchal structure formed from the biomineralization processes is different.

The composite hierarchal structure of bone preforms many diverse mechanical, biological and chemical functions.[5] To understand the macroscopic properties of bone it is important to understand the structural relationship at different length scales. Figure 1.1.1 taken from *Rho, J. Y* shows the hierarchical structure of bone at five different length scales. At the macrostructure, bone can be two different types dense compact bone known as cortical bone or a trabecular rod like structure known as cancellous bones. Bone is made up of osteons, microscopic rods 10-500 um wide consisting of an arrangement of lamellae wrapped together.[5] The lamellae consist of

collagen fibers, in a common orientation and surrounded by mineral to form sheets 3-7 um thick.[5]

Teeth are composed of enamel, dentin, and the dental pulp chamber. Dentin can be of two types either peritubular or intratubular dentin, and intertubular dentin. Dentin forms in a tubular structure, the tubes allow for the transportation of odontoblastic cells, the cells responsible for the formation of dentin. The tubules expand from the dental pulp chamber to the dentin-enamel junction (DEJ) . The intratubular dentin, which makes up the walls of the tubules, is a highly mineralized form of dentin with limited organic matrix.[10] Tubules range from 0.8 um to 2.5 um in diameter and make up between 1% to 22% of the area.[10] The intertubular dentin surrounds the tubules and consists of a extracellular matrix composed of mostly type I collagen reinforced apatite. Figure 1.1.2 shows the structure of a tooth and the densities of the tubules at various points in the tooth. The dental pulp chamber is lined with odontoblastic cells supporting the odontoblastic processes in the tubules. The enamel consists of a more highly mineralized apatite and is formed by ameloblasts. Dentin and enamel have similar mineral environments, consisting of a carbonate rich, calcium deficient Hydroxyapatite.[10] However, dentin and enamel form by very different mechanisms, cells and proteins, leading to a more highly mineralized material in enamel.

1.2 – Implants

On average a person walks one million steps in a year with each step a load change. The load on the joints is roughly 1kN during standing, 2-3 kN while walking, up to 5 kN when running and up to 8 kN during jumping.[15] This results in wear on the joints and with an increasing number of people living longer, becoming increasingly overweight, and living more

active lifestyles the number of people with joint and skeletal problems is on the rise.[15] The

wearing down of the protective tissues around joints is known as osteoarthritis and can cause

pain, tenderness and loss of mobility. There is no known cure for osteoarthritis and as the

condition worsens the only way to regain mobility is with an endoprosthetic implant.

Endoprosthetic implants are used to replace damaged or missing body parts inside the body and

are a solution to restore function and increase the quality of life for a wide variety of problems,

including hip, knee, glenohumeral (shoulder), ginglymus (elbow) and dental implants. Figure

1.2.1, taken from *Heimann, R. B.* shows a typical hip replacement. Traditional hip implants

usually consist of a metallic femoral stem, a metallic or ceramic femoral ball and a metallic

acetabular cup. Failures of these implants are typically due fracture in the bone or cement fatigue

failure causing the need for resetting the implant requiring, further drilling away of the bone to

create a new surface for which the implant can be attached. While these implants can restore

mobility in patients they fall short of returning normal function and the lifespan of these implants

will be outlived in younger patients. In order to increase the lifespan of endoprosthetic implants,

osteointegration between the implant and bone is needed. Osteointegration is the formation of an

interface at the implant and bone without connective tissues.[16]

Current implants are designed for osteointegration by using Hydroxyapatite coatings to

trigger a biological reaction between the surface of the implant and bone.[15] Hydroxyapatite

coatings provide an osteoconductive environment, supporting the growth of capillaries and cells

to form bone.[17] Osteoconductive materials provide a guide for the regeneration of bone in

locations where healing will occur naturally.[17] Eliminating the need for the implant to be

cemented in place and creating a more mechanically stable interface between the implant and

bone. A porous stem with pores on the scale of 100-150 microns is required for the formation of

bone to take place. This is to allow blood flow into the implant to deliver cells to aid in the biological fixation.[18] The increased surface area between the bone and implant also leads to a better fixation of the implant.[19] In order for biological fixation to occur the implant has to remain in place during healing. Micro motion, a shift in the implant position on the micron scale, can cause tissue damage or result in the blood supply being cutoff.[18] Resulting in death of the tissue or inflammation that leads to the implant failure.[18] If an uncemented implant is well osteointegrated it is thought that it will provide a more durable fixation, and avoid the complications of cement fatigue failures allowing for a longer lifespan than cemented implants.[20,21,22]

Dental enamel serves to protect the dentin, unfortunately as it ages and is exposed to various foods and beverages it can degrade or erode, leaving the dentin unprotected. Diseases, infections, and decay can result leading to the loss of the tooth. Additionally, periodontal diseases and receding gum lines can expose the root of the tooth leaving it vulnerable to decay and infection, subsequently leading to loss of the tooth. In these cases a dental implant is needed. A dental implant is an artificial tooth, which is anchored into the jaw, and holds the artificial tooth or bridge in place. Dental implants are permanent and do not rely on the surrounding teeth for support. Dental implants are load-bearing implants made of metallic or a bone-like ceramic material that's compatible with the surrounding body tissues. Teeth are connected to the jaw via the tooth bearing bone, the maxilla for upper teeth and the mandible for the lower teeth. When a dental implant is needed, it is fixated to these bones in order to ensure the implants survival and stability. Osteointegration between the root of the implant and the maxilla or mandible is essential to the implants fixation.

Early fixation of cementless implants is crucial to their lifespan. Failures of cementless implants have been caused, within the first five years, by aspetic loosening, loosening not caused by harmful microorganisms or viruses.[20] To improve the fixation of implants, the materials used must be engineered to provide the maximum biological response, to ensure early fixation of the implant.[20]

1.3 - Enhancing Osteointegration

Immediately following implantation a series of cellular and extra cellular events occur in the healing process. The first interactions of the implant with the body occur at the surface of the implant. It is therefore of crucial importance to understand the role of the microstructure, chemical modifications and topography in the process of bone formation. The first biological components to interact with the implant are blood cells. Platelets in the blood adhere to the surface of the implant and form clots. Biological changes in the cells caused from the interaction of the platelets with the implant surface can result in various biochemical responses. These biological responses allow for the formation of the extra cellular matrix (ECM). The ECM acts as a scaffold for the migration of ostseogenic cells, which induce the crystallization of hydroxyapatite. The more quickly cells adhere to a surface and begin formation of the ECM, the faster the healing process will be.

The use of Hydroxyapatite as a biomaterial has been demonstrated to promote rapid regeneration of bone and allows it to directly bond to regenerated bones without intermediate connective tissues.[18] By coating a cementless implant with hydroxyapatite, the rate of bone regeneration can be increased. Hydroxyapatite coatings are deposited on the implant by thermal spray deposition, a process where heated or melted materials are sprayed onto a substrate. The

crystallinity of Hydroxyapatite coatings must be controlled, highly crystalline Hydroxyapatite is very stable in pH values above 4.3 making it bioinert and inhibiting cell proliferation.[15,23,24] The porosity and topography of the coating will effect the response of osteoclasts, cells responsible for resorbing bone.[25] Osteoclasts are more active when interacting with rough surfaces leading to accelerated bone growth. Pores are also essential to osteoclast absorption, and the osteointegration of the implant.

Aside from the implants coating the materials making up the stem also have to be engineered to aid in osteointegration. The stems surface chemistry and topography are capable of modifying cellular behavior. State of the art implants use a femoral ball made from Yttria stabilized zirconia or alumina and femoral stems made from bioinert Ti6Al4V alloy.[15] Additionally, titiana (TiO_2) has shown potential to be a useful biomaterial, due to its ability to modulate protein interactions.[26] Early studies on titiana implants have shown their potential to accelerate bone growth.[1,26] While it is known that certain surface chemistries and topographies increase the rate of bone regeneration, the relationship of the surface energy to the bone growth is not well understood.[25]

1.4 - Raman Spectroscopy for Biological Apatites

The most common methods used to characterize biomineralization are Fourier transform Infrared Spectroscopy (FTIR), X-ray diffraction, Energy-Dispersive X-ray Spectroscopy (EDX), X-ray Photoelectron Spectroscopy (XPS) and Scanning Electron Microscopy (SEM). FTIR is commonly used in vibrational spectroscopies, although the sample preparation requires the pulverization of the sample to a powder for analysis, which often results in foreign substances introduced to the samples that change the results.[27] EDX and XPS give information on the

chemical compositions of a sample but fail to provide information on the molecular level. X-ray

diffraction can give information on the crystal structure and chemical bonds present in a sample.

Biological analytical techniques, such as morphological and histological staining are used

to test for the presence of certain chemicals or ions, for biominerals stains are used to detect

calcium. Hundreds of stains are available to test for a variety of cellular components and

proteins. Stains are designed to bind with specific molecules or ions that they have a high affinity

for. Once bound to the desired ion they can be seen using optical microscopy or in some cases

fluorescence microscopy. However these tests are only able to provide information if a species

is present.

Due to the complex structure of bone, a more in depth material analysis is needed to fully

understand the structure.[9,23] Raman spectroscopy has been identified as a technique that is able to

provide insight to the structure of biomineralized deposits and the differences between

engineered biomineralized deposits grown from different cell lines compared to native bone and

study the mineralization process. Another major advantage of using Raman spectroscopy is it is

able to identify and characterize elements and molecules, an important advantage when studying

composite biominerals.

1.5 – Raman

When light interacts with matter it will be absorbed reflected or scattered. In cases where

the photons is scattered, three possibilities exist. The most common way a photon scatters is

known as Rayleigh scattering, where the incident and scattered photon are equal in energy also

called elastic scattering. Inelastic scattering occurs when there is an energy change between the

incident and scattered photon. Inelastic scattering is a much less common occurrence with only

about one in 10^6 to 10^8 incident photons scattering inelastically.[27] Figure 1.5.1 shows the different scattering possiblities. In these interactions the incident photon is eliminated and a new scattered photon is produced.[28,29] The energy difference between the incident and scattered photon is equal to the energy difference between the excited and ground states of a molecule, this is the basis of Raman spectroscopy.

Irradiation of a sample causes polarization of the electron cloud, a short-lived virtual electronic state is created. The energy level of the virtual states is dependent on the light frequency used for irradiation. Raman scattering from these virtual states can occur two ways. In Stokes scattering energy from the incident photon is absorbed by a ground state, promoting it to an excited energy level, and the resulting scattered photon is lower in energy. If the material is already in an excited state, a transfer of energy from the material to the photon occurs and the scattered photon is higher in energy, known as anti-Stokes scattering. Since most materials are in the ground state at room temperature, the Stokes scattering process is predominantly used for Raman analysis. Anti-Stokes spectra are used mainly for analysis of materials with large fluorescence bands in the Stokes region. In order for a sample to be Raman active it has to be polarizable, therefore metals and other conducting materials are not Raman active.

The use of Raman for characterization of a material is dependent on the change brought about by the activation of a vibrational mode, due to the change in polarization. The change in polarization can be caused by a change in the size or orientation of the atoms in the crystal structure. Vibrational frequencies are dependent on the position of the atoms and the interatomic forces between the atoms. Therefore using Raman the crystal structure and its orientation can be determined, as well as information about the order and strain in the material. In a Raman spectra a change in the peak position, is indicative of a change in stress in the crystal structure. Stress

will change the distance between bonds in a crystal structure and therefore the vibrational frequency. The crystallinity or order of a crystal structure can also be determined from Raman spectra, as an increase in the disorder will result in bonds of varying distances. Therefore the width of the peak is correlated to the distribution of the average bond distances in the sample. Hence, a greater peak width is characteristic of a disordered crystal structure.

Laser frequency selection is vital to obtain high quality Raman spectra. The intensity of the Raman signal is proportional to the polarizability of the material and frequency of the laser according to the equation. [11]

$$I = Kl\alpha^2\omega^4$$

Where I is the intensity of the Raman signal, l is the laser power, α is the polarizability of the sample and ω is the frequency of the laser light. While this equation would suggest that a high frequency laser such as UV should produce more intense spectra, this is not always the case. High-energy photons may also damage fragile samples such as biological tissues and polymers by so called "burning" photon damage at the surface.[27] The choice of visible laser excitation, although less prone to both of the challenges above, may excite fluorescence in samples which can overwhelm the Raman signal making it impossible to obtain useful data. In these studies infrared laser radiation can often address both of these issues. The lower energy of this laser is used to avoid excitation luminescence from many biological and polymeric materials, while also avoiding the damaging effects of higher energy light.[30]

Compared to FTIR spectroscopy, Raman offers the advantage of having little to no sample preparation which can alter the samples chemical composition. Being an optical microscopy technique, it allows for the sampling of microscopic regions of the sample. This provides the ability to analyze very small regions. Mapping experiments where multiple Raman

spectra are obtained from a region of the sample allows for the analysis of the change in chemical environment in a region of the sample. The Raman spectrometer is equipped with a motorized XYZ stage, which after completing a scan will move, and start a new scan allowing for spectra to be collected over an entire region of a sample, step sizes can be controlled down to 50 nm.

1.6 - Raman Spectra of Apatite Biominerals

Biominerals such as bone, dentin, and enamel all result in similar Raman spectra. A Raman spectrum of the upper incisor of a native mouse tooth is shown in figure 1.6.1. The spectrum is dominated by the v_1 PO_4^{3-} vibrational band characteristic of Hydroxyapatite, occurring near 960 cm^{-1}.[4,23,31] Two other Raman bands associated with Hydroxyapatite occur in the 370 – 500 cm^{-1} region and the 540 – 630 cm^{-1} region representative of the v_2 PO_4^{3-} and v_4 PO_4^{3-} vibrations of Hydroxyapatite, respectively.[4,23,31] The Raman band at 1070 cm^{-1} represents a carbonate substitution in the Hydroxyapatite matrix. [4,23,31] Raman signals relating to phenylalanine can be seen near 650, 1045, 1581 and 1598 cm^{-1}. Protein bands corresponding to the amide I and amide III bands are present in the 1200 – 1350 cm^{-1} and 1650 – 1700 cm^{-1} region, respectively. [4,23,31] Raman bands corresponding to the CH_2 wag of proteins are noticed around 1450 cm^{-1}.[9] Also visible is a large Raman signal in the 800 – 900 cm^{-1} region corresponding to the C-C stretching modes.

2.0 - Experimental

To determine the chemical composition of the samples a Renishaw Raman microscope, equipped with a Leica microscope with the option of standard or high confocal microscopy. The system is controlled with Renishaw Wire 3.2 software. Laser irradiation was emitted using a solid state AlGaAs laser producing a monochromatic beam at a wavelength of 785 nm. Two different model lasers were used an Innovative Photonic Solutions (Model # I0785SR0100B) with a spectral width of <0.001 nm and an output power of 100mW, and a Reinshaw (Model # HPNIR785) laser with a spectral width of 0.25 nm and a output power of 350 mW. Additionally a multi-wavelength Argon gas laser was used for scans using a 514 nm wavelength, made by Modu-laser (Model Stellar-REN) with an output power of 150 mW. For data collected with the 785 laser, a 1200l l/mm grating was used with a blaze coating for 600-780 nm, and a 785 nm edge filter. For the 514 laser, a 1800 l/mm grating was used, blazed for use with visible light in junction with, a 514 nm edge filter. Data was collected using an air-cooled silicon CCD detector..

The data was processed using Renishaw Wire 3.2 or 4.0 software. For the mapping experiments the integral to the area under the spectra was normalized to one before further analysis. The spectra were curve fitted using Gaussian – lorentzian curves, after curve fitting a single spectrum; parameters can be saved and applied through all the scans collected in the mapping experiment.

2.1 – Mouse tooth - samples

Mice teeth samples were obtained for investigation by Raman spectroscopy. These teeth exhibited a white stripe of irregular dentin on the inside of the upper and lower incisors as seen in figure 2.1.1. The chemical composition of these teeth was investigated by Raman

spectroscopy using a 785 nm laser. The teeth were removed from the mouse jaw and mounted in crystal bond. A Raman mapping scan was performed using a 50x magnification with standard confocality, over the 300 cm^{-1} to 2000 cm^{-1} region, to investigate the changes in chemical composition over the area of irregular dentin. To obtain high signal to noise spectra it was necessary to use long scan times with high laser power, however the prolonged exposure of the laser on the sample leads to sample degradation through burning, especially during the mapping experiments. In order to overcome sample burning in this experiment the scan time was reduced, by using larger step sizes between scans and shorter scans. Low magnification measurements of the irregular dentin region revealed less mineralization and gave a spectra dominated by Raman bands associated with organic material. After identifying the correct region to scan higher magnification scans were preformed. Two areas of the teeth were chosen, one containing the irregular dentin near the tip of the tooth, and the second was performed on the irregular dentin lower down on the tooth away from the tip, to ensure the change in the chemical structure wasn't due to erosion of the tooth by wear during mastication.

Spectra were curve fitted in three regions, the 300 to 800 cm^{-1}, 800 to 1200 cm^{-1} and to 2000 cm^{-1}. In the 300 to 800 cm^{-1} region Raman bands due to the v2 and v4 vibration modes of phosphate are present, at 422 to 454 cm^{-1} and 578 to 617 cm^{-1} regions, respectively, they were fitted each with 3 peaks and another single peak at 650 cm^{-1} was observed in some spectra, which was fit with one peak. The 800 cm^{-1} to 1200 cm^{-1} region consisted of many peaks, of varying intensities depending on the region of the tooth, in the mineralized region the 960 band dominated the spectra, while in the irregular dentin the spectra was dominated by organic absorptions in this region. In order to fit this region a mineralized spectra was first fitted, and the peaks were pinned to ±2 cm^{-1}, this fitting was then applied to a non-mineralized spectra where

the organic bands were better represented, and they were fitted and pinned. Lastly the 1200 to 1800 cm^{-1} region was fitted from a spectrum of the non-mineralized region and pinned to ±5 cm^{-1}. After applying the curve fitting to the entire map, data was generated on the mineral to matrix ratio, carbonate to phosphate ratio and the width and position of the v1 phosphate peak.

2.2 – Human Teeth Samples

The interface between dentin in enamel, commonly referred to as the dentin enamel junction (DEJ), is not fully understood. Raman mapping scans were used to investigate the chemical composition of this junction to provide a better understanding of the chemical environment present in this region. Two samples, a permanent tooth and a deciduous tooth, commonly called a baby tooth, were investigated. The tooth samples were cut longitudinally, mounted in crystal bond and polished from a 240 grit sand paper down to a 0.3 micron finish using an alumina solution and a polishing cloth. Data was collected using high confocality microscopy and 785 nm laser operating at 350 mW. A one micron step size and 120 second scan time were used to obtain a high resolution scans and mapping experiments in the 300 to 2000 cm^{-1} region. Due to the larger area of the samples the higher power and long scan times did not lead to sample burning.

High-resolution scans were obtained around the DEJ. The scans revealed many peaks in the 300 to 2000 cm^{-1} range and the spectra were curve fitted by choosing scans from the DEJ, which showed large amounts of organic components. Like the mouse tooth samples the curve fitting took place in 3 regions. The 300 to 800 cm^{-1} region which contained peaks corresponding to the v2 and v4 modes of phosphorus and a peak corresponding to phenylalanine. The 800 to 1200 cm^{-1} region was curve fitted for all peaks present, especially the peaks corresponding to the v1 phosphate mode, amorphous phosphate, carbonate substitution and collagen. The last region

1200 to 2000 cm^{-1} was curve fit for all the peaks present including the amide III and I bands, the CH2 wag, and the two peaks corresponding to phenylalanine. All peaks were fitted and pinned to their position,

2.3 – Dental Stem Cells

Research in this area involves the growing of biominerals through the use of cells. While some cell lines are known to produce mineralized tissues, a materials analysis is needed to determine how similar minerals grown from cells are to native biomineral tissues. Dentin grown from six different cell lines of PDL, SCAP, SHED, BCMP, DPA and GF on magnesium fluoride substrates were investigated using Raman microscopy and compared to native dentin.

After cell culture the samples were boiled in distilled water for 1 hour to remove C-H bonds the were created on the surface and then placed in a 70% ethanol solution for 30 minutes to ensure sterilization.

Mineralized nodules were apparent under 5x magnification, in order to choose which areas to scan, quick static scans were preformed to see if the 960 cm^{-1} phosphate peak was observed. If present a higher quality 20x mapping experiment was preformed. The magnesium fluoride, substrate has large Raman bands in the 1000 to 1800 cm^{-1} region, which overlap the organic region of biominerals. These bands were apparent under in both confocal and standard confocality modes. Mapping experiments were taken to observe the 300 to 2000 cm^{-1} region. Due to the samples vulnerability to burning, lower laser powers and multiple accumulations of scan points were used in the mapping experiments, sacrificing the ability to obtain higher resolution spectra. To obtain higher resolution scans single point scans were taken using higher laser power and longer scan times, points were chosen in the center of the mineralized nodule, near the edge of the nodule and on the substrate.

Data analysis was preformed by curve fitting the 800 to 1200 cm^{-1} region, peaks corresponding to the phosphate, and carbonate are apparent in this region. The 960 band typically overlaps with an ~950 cm^{-1} band, corresponding to an amorphous phosphate of much power intensity. Curves were pinned to ± 3 cm^{-1} of the observed peak in order to insure the proper peak fitting when applying it to the rest of the data collected in the mapping experiment. The organic region, 1200 to 1800 cm^{-1} was peak fitted by first peak fitting the spectra of only the substrate and then applying that peak fitting to a spectra obtained from the nodules and then curve fitting the organic peaks corresponding to the amide I1600-1720 cm^{-1} and CH2 ~1450 cm^{-1}, again these peaks were pinned to ± 5 cm^{-1} to ensure they related to the proper peaks, when applying the curve fit to the rest of the data collected.

Data analysis consisted of relating the area of the mineralized 960 cm^{-1} peak to the area of the Amide peak in the 1600-1700 cm^{-1} region, in order to determine the mineral to matrix ratio. The peak around 1070 cm^{-1} corresponds to the carbonate peak and the ratio between the carbonate and 960 cm^{-1} phosphate peak was used to determine the carbonate to phosphate ratio. A ratio between the amorphous phosphate and 960 cm^{-1} peak was also calculated. Further analysis of the spectra included the change in the width and position of the 960 cm^{-1} peak over the mapping area.

2.4 – Hydroxyapatite Coatings

Hydroxyapatite coatings were obtained for use in future experiments, Raman spectra for these coatings was obtained to determine information of the amount of crystallinity, stress and chemical composition of these samples. A large extended scan from 100 to 3200 cm^{-1} was preformed to determine where the peaks of interest were. The only peaks observed were due to the phosphate content and the region 900 to 1200 cm^{-1} was scanned. This region only exhibited

2 peaks, which were fitted. For these scans the 514 nm laser was used and a step size of 1 micron by one micron.

2.5 – TiO2

Various heat-treated titanium oxide substrates were incubated for 14 days, in bone marrow-derived stem cells, MC3T3 of mice. After cell culture the samples were boiled in distilled water for 1 hour to remove C-H bonds the were created on the surface and then placed in a 70% ethanol solution for 30 minutes to ensure sterilization. The heat treatment of the substrates changes the surface free energy, in order to determine the relationship between the surface free energy and the cells behavior these samples were investigated using Raman spectroscopy.

Titanium oxide samples heat-treated at 300C, 400C, 600C and 800C and one sample left at room temperature were analyzed. Titanium oxide has a strong Raman signal below 900 cm^{-1}. In order to obtain quality spectra where the Raman signal due to the biological materials the 900 to 2000 cm^{-1} region was scanned. Since bone nodules do not start to form mineral until after 14 days in culture, the Raman spectra showed signals relating to the organic component only. Raman scans were done using a 785 nm laser and 1200 grating, using the high confocality mode. Step sizes were consistent at 2.5 microns throughout all the samples.

A Raman mapping experiment was preformed on all these samples. To avoid sample burning and still obtain useful spectra scan times were kept short. High confocal scans at 50x magnification were used. The points of interest on the samples were relatively small. All scan times were 10 seconds, and used a step size of 2.5 x 2.5 microns. The mapping consisted of 40-70 accumulations.

3.0 - Results and Discussion

3.1 - Mice teeth

White light images of the mice teeth exhibiting the white stripe of irregular dentin on the upper and lower incisors, near the tip of the tooth and away from the tip of the tooth, as well as the areas investigated by Raman are shown in figure 3.1.1. Characteristic Raman spectra corresponding to different areas in the tooth are shown in figure 3.1.2. Spectra corresponding to areas of regular dentin were dominated by Raman bands characteristic of Hydroxyapatite. Peaks of the organic components and collagen corresponding to the extra cellular matrix were also present although in lesser intensities. In the areas of irregular dentin the organic components and collagen had a greater presence in the spectra. All the teeth showed a lesser degree of mineralization present in the areas of irregular dentin, determined by the mineral to matrix ratio. However the presence of amino acids in some areas of the irregular dentin samples as well as collagen suggest these areas may be in the process of mineralization.[2]

The mineral to matrix ratio plotted as a function of position can be seen in figure 3.1.3. In areas of regular dentin the mineral to matrix ratio varied from 4.0 to 4.5 depending on the distance from the irregular dentin. In the upper and lower incisor scans near the tip a gradual increase in the mineral to matrix ratio moving from the area of irregular dentin to regular dentin was observed on one side of the white stripe. This suggests these areas are further along in the mineralization process. While on the other side of the white stripe a more drastic increase in the mineral to matrix ratio was detected. The upper incisor near the tip showed the mineral to matrix ratio increasing to 3.5 and above with in 5 microns of the stripe on the right side of the stripe and on the left side the mineral to matrix ratio is only around the 1.5 range 5 microns out on the left side. In the lower incisor near the tip this was also observed with the mapping region in the

bottom left an increase in the mineral to matrix ratio immediately outside of the irregular dentin region to 4.5. On the right of the side of the mapping region the mineral to matrix ratio was observed to increase slowly to about 3. In the upper and lower incisors away from the tip of the tooth a mineral to matrix ratio of 3.2 and 4.5 were observed in the areas of regular dentin immediately outside of the white stripe. In the areas of irregular dentin, a range of mineral to matrix ratios was observed.   In the lower incisor near the tip of the tooth a higher mineral to matrix ratio was observed to be 0.5 in a few spots, but closer to 1.8 over the majority of the area or irregular dentin. In the lower incisor away from the tip the area of irregular dentin had areas where no mineral was detected, and a mineral to matrix ratio of 0.5 in other areas. In both of the mapping regions of the upper incisor a mineral to matrix ratio of 0.5 was observed in the areas of irregular dentin.

An increase in collagen content is observed in the areas of irregular dentin compared to the areas of regular dentin. A map of the area under the collagen peak is shown in figure 3.1.4. Varying amounts of collagen occur throughout the areas of irregular dentin and there appears to be no correlation with the changes in the mineral to matrix ratio in these regions. In the upper incisor near the tip the collagen presence is greatest in the areas of irregular dentin in three clusters, and has little presence in other areas of the irregular dentin. On the left side of the sample, where the mineral to matrix ratio slowly increased moving out from the irregular dentin, a slow decrease in the amount of collagen present was detected. However on the lower incisor near the tip the collagen presence is increased in the area of irregular dentin on the right side, where an increase in the mineral to matrix ratio was also observed. In the upper incisor away from the tip the collagen presence was observed to be much higher in the areas of irregular dentin, and like in the upper incisor sample near the tip, its presence is not consistent throughout

19

the region but in distinct clusters. The lower incisor away from the tip also showed a large

presence of collagen in some areas of the irregular dentin, although there was an almost equal

presence in the area of regular dentin. From the maps of the collagen it appears that the collagen

forms in clusters, in the areas of irregular dentin, possibly the beginning of a scaffold for the

mineralization of these areas. Although the upper and lower incisors near the tip of the tooth

showed a contradictory correlations between the mineral to matrix ratio and the amount of

collagen, they could be at similar stages of mineralization, where collagen provides the

framework for the beginning of mineralization, and as its removed in the mineralization process.

The Raman maps from the upper incisor away from and near the tip both showed peaks

corresponding to an amino acid phenylalanine, shown in figure 3.1.5. The phenylalanine

presence in the upper incisor is most concentrated in the areas of the irregular dentin where there

was less collagen present. On the upper incisor away from the tip there were two distinct clusters

of higher collagen content, the phenylalanine in this sample had the highest presence in the

collagen cluster closest to the regular dentin, while in the second cluster of collagen the presence

of phenylalanine had decreased. Phenylalanine has a high binding affinity for hydroxyapatite

and is believed to play an important role in directing hydroxyapatite crystals into the collagen

scaffold for mineralization.[32]   The observations of the phenylalanine in areas of high

mineralization and low collagen content as well as in areas of high collagen content and low

mineral suggests that the collagen scaffold is first conducted, followed by an increase of

phenylalanine to bring hydroxyapatite in for mineralization along with the removal of the

collagen content.

A more in-depth analysis of the mineral component of the mice teeth over the area of

irregular dentin was investigated to provide further insight on the mineralization hydroxyapatite

happening in this region. The amount of carbonate substitutions was determined by the carbonate to phosphate ratio and is plotted as a function of position in figure 3.1.6. In the upper incisor near the tip the mineralized dentin areas gave a value of 0.12 for the carbonate to phosphate ratio. However in the irregular dentin area, the values varied between 0 and 0.05 in most areas. There were two spots with a carbonate to phosphate ratios between 0.18 to 0.27. This may be due to poor curve fitting from Raman bands which overlap with the carbonate peak, making it difficult to accurately quantify the signal. Away from the tip of the upper incisor the carbonate to phosphate ratio was found to be 0.27 for mineralized dentin and in the area of irregular dentin the carbonate to phosphate ratio varied, from 0.05 to 0.15, the increased amount of carbonate substitutions occurred in the same area that had a larger collagen component and little phenylalanine present. Studies have indicated that the carbonate in hydroxyapatite helps absorb proteins and cause cells to differentiate,[14] further supporting that this region is at an earlier stage in the mineralization process than observed in the other cluster of collagen. The carbonate to phosphate ratio in the lower incisor near the tip of the tooth was observed to be 0.1 in the areas of regular dentin and in the areas of irregular dentin the carbonate to phosphate ratio varied between 0.05 to .22, with the higher points of carbonate substitution also present where an increase of collagen was detected, as in the previous sample. The lower incisor away from the tip the carbonate to phosphate was found to be 0.3 in the areas of regular dentin, while in the areas of irregular dentin a higher presence of carbonate was detected and found to be as high as 1.0 in some areas, although there may be some error in this ratio as the phosphate peak can barely be detected in the irregular dentin in this sample.

Another mineral environment in the dentin mineral is present in the form of an amorphous phosphate species. To quantify the amount of amorphous phosphate present a ratio

of the amorphous phosphate to crystalline phosphate was calculated by using the v1 phosphate peak and the amorphous phosphate peak at 950 cm^{-1}, shown in figure 3.1.7. The amorphous phosphate peak is appears within the v1 phosphate peak. In the upper incisor near the tip of the tooth he amorphous phosphate to crystalline phosphate showed a consistent ratio of 0.25 in both the irregular and regular dentin. In the upper incisor away from the tip of the tooth there does appear to be a difference in the amount of amorphous phosphate present in the irregular dentin area of the tooth as seen in figure 3.1.8, which shows the ratio between the amorphous phosphate and crystalline phosphate present. As seen in the figure the amount of amorphous phosphate is higher in the irregular dentin area when compared to the mineralized areas. Within the area of irregular dentin there appears to be a correlation between the amount of amorphous phosphate and the amount of phenylalanine and collagen. In the larger cluster of collagen without phenylalanine a higher ratio of amorphous phosphate to crystalline phosphate was observed at 0.6, while in the collagen cluster with the phenylalanine the ratio of amorphous phosphate to crystalline phosphate is equivalent to the ratio observed in the mineralized dentin at 0.25. In the lower incisor near the tip of the tooth the ratio between the amorphous phosphate and crystalline phosphate was found to be consistent at 0.25 across the entire mineralized region. In the areas of irregular dentin the 960 peak was observed at very low intensities overlapping the amorphous phosphate preventing the ratio from accurately being determined. In the last sample in the lower incisor near the tip the ratio of the amorphous phosphate to the crystalline phosphate was found to be 0.22 in the areas of regular dentin. While in the area of irregular dentin this value varied between 0.1 to 0.22.

The last analysis's preformed on the mineral component of the teeth was the change in the v1 phosphates peak position and width. Changes in these values indicate an increase in the

disorder of the crystalline component, as the peak widens. The change in the peak position is indicative of a change in stress. Figure 3.1.9 shows the position of the v1 phosphate peak as a function of position, and figure 3.1.10 shows the peak's width as a function of position. The analysis of the v1 phosphate peaks position in the upper incisor near the tip shows no significant change throughout the mineralized and irregular dentin area, observed at 960.4 cm^{-1}. Which indicates a similar amount of stress in the Hydroxyapatite matrix throughout the tooth. The peak width of the v1 phosphate peak also remained consistent throughout both regions in the tooth, with a width of 15.8 cm^{-1}, the consistent width implies that hydroxyapatite mineralizes and matures without much change in the crystal structure. In the upper incisor away from the tip, the peak position of the 960 cm^{-1} peak also was not effected in the region of irregular dentin, giving a consistent position at 960.4 cm^{-1}. Although an increase in the amount of amorphous phosphate was observed it didn't affect the width of the 960 cm^{-1} peaks, which were consistent at 15.8 cm^{-1} throughout the entire mapping region. In the lower incisor near the tip the position of the v1 phosphate peak also remained constant, appearing consistently at 960.1 cm^{-1}. The width of the 960 did show a slight change over the mapping region. In the areas of mineralized dentin the peak width was observed at 15 cm^{-1}, where as in the regions of irregular dentin a peak width between 17 and 19 cm^{-1} was observed. The change in peak width indicates the Hydroxyapatite mineral component in the irregular dentin region is less ordered or crystalline than that found in the areas of regular dentin. A more disordered Hydroxyapatite component could be indicative of the mineral in a very early stage in the mineralization process, where the Hydroxyapatite is still being brought into the matrix preceding the crystals growth. The v_1 phosphate peak was observed at 960.8 cm^{-1} with no significant change in the position. The peak width of the v1 phosphate peak was also observed to remain consistent throughout the sample at 14.1 cm^{-1}. The

consistency of the v1 phosphate peak indicates the stress in the crystalline component of the dentin remains the same through out the entire sample. The upper incisors had the same stress and crystalline order throughout the mapping region, where as the lower incisor had a slight increase in the crystalline component moving down the tooth, accompanied by a slightly more stressed crystalline structure.

The extra cellular matrix, is composed of various organic compounds comprised mostly of amino acids. The amide I peak of these amino acids can provide information about the stress and order in the extra cellular matrix. The position and width of the amide I peak was plotted as a function of position in figures 3.1.11 & 3.1.12, respectively. Analysis of the amide I peak width in the upper incisor near the tip, shows a consistent width across the entire mapping region of 52.2 cm^{-1}. Suggesting that the matrix component of the tissue retains a similar amount of order in the mineralized region and region of irregular dentin. The peak position however was found to shift between 1651 and 1672 cm^{-1}, indicating a change in stress throughout the tooth. In the area of irregular dentin the peak position of the amide I peak was lower than that observed in the areas of mineralized dentin. A smaller shift in the peak position around 7 cm^{-1}, was observed inside area of irregular dentin area as well. On the right side of the image, the area where the phenylalanine peaks are observed, the amide I peak is observed at lower values around 1657 cm^{-1} where as in the area towards the left of the irregular dentin the peak is observed around 1662 cm^{-1}. The peak width of the amide I peak of the upper incisor away from the tip was found to be consistent at 48 cm^{-1} in the area of regular dentin. While in the area of irregular dentin the width of the amide I peak was larger and varied between 51 to 58 cm^{-1}. Indicating there is less order in the organic component of dentin. The peak position of the amide I peak also showed some variation when observed in the area of irregular and regular dentin. In the area of irregular

dentin the amide I peak occurred at a lower value at 1661 cm^{-1}. In the area of regular dentin the amide I position was observed at 1670 cm^{-1}. Analysis of the amide I peaks position in the lower incisor near the tip occurred between 1655 and 1665 cm^{-1}. In the area of irregular dentin the amide I position occurred at 1665 cm^{-1} where as in the areas of regular dentin the amide I peaks position occurred consistently at 1655 cm^{-1}. In the lower incisor away from the tip the peak width ranged from 65 to 95 cm^{-1}, in the area of mineralized dentin the peak width was consistent at 65 cm^{-1}. In the areas of irregular dentin the width varied from 65 cm^{-1} to 95 cm^{-1}. The area's furthest from the regular mineralized dentin had the largest peak widths. This indicates there is less order in the organic component in this region suggesting that the ECM could still be in the process of forming. The ECM formation is an early step in the mineralization process and the increased disorder in this region reinforces this conclusion.

Areas of irregular dentin were present in all the mouse tooth samples at multiple regions in the tooth. These areas were along a white stripe that ran longitudinal on the inside of the tooth and were determined to have a lesser degree of mineralization, by comparison of the mineral to matrix ratio, determined by the ratio of the area of the v1 phosphate band to the area of the amide I band. In the samples with the lower degrees of mineralization the mineral to matrix ratio was determined to be around 0.5, these areas also exhibited peaks characteristic of phenylalanine, an amino acid hypothesized to play a role in the formation of hydroxyapatite in mineralized tissues due to its high binding affinity. Both areas examined by Raman in the upper incisor sample, had similar mineral to matrix ratios and both showed phenylalanine present. Phenylalanine appears to be present in greater concentrations in areas where the collagen presence is also larger. Indicating these areas, are probably nucleation sites for the growth of biomineral. In the areas of irregular dentin in the lower incisor there no phenylalanine was detected. However in these areas

had different mineral to matrix ratios of 1.8 for the lower incisor near the tip and 0-0.5 in the lower incisor away from the tip. The lack of phenylalanine presence could indicate these areas are in even different stages of mineralization, where the phenylalanine had already initiated the mineralization of Hydroxyapatite, in the sample with a greater mineral to matrix ratio, and in the other sample may have been observed in the stages before the phenylalanine, comes into the biomineral.

3.2 Human teeth
3.2.1 Adult PT sample

A white light image of the dentin enamel junction investigated in this experiment can be seen in figure 3.2.1 with spectra from different points from the mapping experiment. The mapping area included scans along the dental enamel junction as well as scans in the dentin and enamel. The spectra are dominated by the v1 phosphate peak throughout all the mapping regions. Spectra from the enamel region only show peaks corresponding to the vibrational modes of phosphate and a carbonate substitution. Peaks corresponding to the organic components of the mineral were not visible in the spectra for the enamel and the mineral to matrix ratio could not be determined. In the region corresponding to the dentin peaks corresponding to the organic component of the biomineral where present with very low intensities, making the curve fitting for this region problematic. The area of these peaks couldn't accurately be determined so the mineral to matrix ratio could not be determined for this region. The low intensities from the organic component could be due to the sample preparation. The polishing of these samples prior to Raman investigation may have removed some of the organic components in the sample.

In the dental enamel junction peaks corresponding to phenylalanine were observed. As well as peaks corresponding to the organic components of the CH_2 wag, amide I and amide III. However a large peak shift was observed for the amide I band which was observed at 1731 cm^{-1}, which was usually observed around 1680 cm^{-1}. This shift suggests a significant change in the stress of the organic matrix in this region.

Figure 3.2.2 shows a map of the carbonate to phosphate ratio through the Raman mapping region. The carbonate substitution is greater in the dentin region than the enamel region and is observed at a ratio of 0.18 compared 0.10 in the enamel region. In the DEJ the carbonate to phosphate ratio seemed to be consistent with that observed in the dentin. The ratio of amorphous phosphate to crystalline phosphate was also calculated and can be seen in figure. In the enamel the ratio of amorphous to crystalline phosphate was found to range between 0.35 and .5, and in the dentin similar values were observed ranging from 0.25 to 0.5. The DEJ however showed a much lower ratio for the width a value of 0.1 throughout the entire region.

An analysis of the peak position of the 960 phosphate peak revealed a slight difference in peak position. In the enamel the 960 phosphate peak was observed at 961.8 cm^{-1} compared to 962.8 cm^{-1} in the dentin. The peak position is often used to determine the amount of residual stress in the sample; the observation of the 960 peak at a higher wavenumber in the dentin indicates more stress present in the sample. In the dental enamel junction the 960 peak was observed at 962.0 cm^{-1}.

An analysis of the 960 peak's width can be seen in figure 2.1.1. In the enamel the peak was observed to be narrower than in the dentin with a peak width of 12.0 cm^{-1}, compared to 13.0 cm^{-1} for the dentin. The DEJ showed the widest peak for the mineral having widths ranging

from 13.0 to 14.0 cm^{-1}. The wider peaks observed in the DEJ indicate a less ordered crystal structure of the Hydroxyapatite, suggesting mineralization is occurring in this region.

No 1003cm^{-1} peak was observed in any of the spectra, indicating a lack of collagen in the mature tooth. The 1003 cm^{-1} peak is typically much smaller than that of the 960 peak, and because of the lack of an intense organic component in the spectra the collagen peak's intensity could be to low to detect. The observation of the Raman bands corresponding to phenylalanine in the DEJ as well as a more intense organic component suggest that mineralization could be occurring in this area to regenerate damaged mineral.

3.2.2 Deciduous Tooth

The Raman mapping region of the DEJ is shown over the white light image in figure 3.2.1, also shown is spectra characteristic of the enamel, dentin and DEJ. The Raman spectra were consistent with that of the adult PT tooth, except in the DEJ region where there were no Raman bands corresponding to an organic component. Again the enamel region consisted of spectra with little organic components detected, while slightly more intense organic peaks where observed in the dentin region. An analysis of the carbonate to phosphate ratio, amorphous phosphate to crystalline phosphate and of the 960 peaks position and width was carried out.

The carbonate to phosphate ratio over the mapping region is shown in figure 3.2.3. The carbonate substitution doesn't vary much between the enamel and dentin, the carbonate to phosphate ratio was found to be 0.11 in both areas. However in the DEJ and the dentin and enamel near this interface had a slightly higher amount of carbonate substitutions with a value of 0.12. Although the carbonate to phosphate ratio did not vary between the enamel and dentin a greater difference was observed in the amount of amorphous phosphate to crystalline phosphate.

The ratio between the amorphous phosphate peak and crystalline phosphate peak can be seen in figure 3.2.3. It can be seen in the enamel has a lower amount of amorphous phosphate present compared to the dentin, with values of 0.07 and 0.11 respectively. The amount of amorphous phosphate appears to slowly increase from the enamel to dentin with a value of 0.09 in the DEJ. To further investigate the structures of the tooth in this area an analysis of the peak position and width of the v1 phosphate peak was performed.

The map of the v1 phosphate peak over the Raman mapping area can be seen in figure 3.2.3a. From Figure 3.2.3b it can be seen that the enamel has a width of 13.00 to 13.15 cm^{-1}, compared to 3.15 to 13.30, indicating that the enamel is a slightly more crystalline region. Moving from dentin to the enamel the crystallinity increases, as it gets closer to the DEJ, and subsequently decreases in the DEJ, which has crystallinity with a similar to that of the dentin, width of 3.15 cm^{-1}. Moving away from the DEJ towards the enamel the crystallinity increases until it reaches the enamel and then gives a constant peak width of 13.00 cm^{-1}.

A slight variation in the peak position of the v1 phosphate peak was also observed over the sample area. Figure 3.2.3 shows the variation of the peak position over the sampled region. As seen in figure 3.2.3 the peak position of the v1 phosphate varied slightly over the mapping region. Moving from the dentin to enamel a decrease in the peak position was observed. In the dentin region a the peak was observed at 961.7 cm^{-1} and slowly decreased across the DEJ to the enamel, and was observed at 961.4 cm^{-1} in the region corresponding to the enamel. This decrease indicates a slight change in the stress of the Hydroxyapatite in the different areas of the tooth. The crystal structure of Hydroxyapatite appears to have a slightly higher amount of stress than that of the enamel.

29

Unlike the DEJ in the permanent tooth their was no signs of an organic component in the DEJ of the deciduous tooth. This could indicate a lack of regenerative properties in these teeth, or could be cause from pullouts of the sample when polishing.

3.3 Dental Stem Cells

The Raman mapping regions as well as the white light image of the mineralized nodules can be seen in figure 3.3.1. Large Raman bands from the magnesium fluoride substrate are seen in the 1200-1800 cm^{-1} region, making it difficult to accurately curve fit the organic components in the samples, a spectrum of the magnesium fluoride substrate can be seen in figure 3.3.2. However the Raman bands due to the CH$_2$ wag and amide I are detectable, the amide III band which occurs at approximately 1200 cm^{-1} is at the peak of the magnesium fluoride band and cannot accurately be determined. All cell lines grew mineralized nodules exhibiting the characteristic v$_1$ phosphate peak of hydroxyapatite, as well as bands corresponding to the organic components.

A characteristic spectrum from each cell line is also shown in figure 3.3.3. All spectra showed peaks characteristic of native dentin, dominated by the v$_1$ phosphate peak. The carbonate peak at 1070 cm^{-1} was also visible in most of the spectra. In the DPA and SHED cell lines, the carbonate peak was not visible due to the dominance of the Raman signal by the substrate. This could be due to the mineralized nodule being very thin. Further analysis of the mineral to matrix ratio, carbonate to phosphate ratio and amorphous phosphate to crystalline phosphate was completed for a more indepth analysis of the mineralized nodules, and can be seen in table. The width and position of the v$_1$ phosphate peak was also analyzed.

The mineral to matrix ratio was for the different cell lines revealed a wide range of values for the different cell lines. The mineral to matrix ratio maps for each cell line is shown in figure

3.3.4. In all the samples the highest points of mineralization occurred away from the edges of the sample. In the mineral formed from the PDL cell line points of high mineralization occurred through out the sample with a ratio of 4.2, while other areas in the nodule showed almost no mineralization. A mineral to matrix ratio of 2.5 to 3.0 was found in between the areas of the high and low mineralization and occurred over the largest area in the sample. The edges of the PDL sample showed almost no mineralization. In the mineral formed from DPA cell line there appeared to be areas where high mineralization occurred. In the top right of figure 3.3.5 the DPA mineralized nodule has a value of 2.3, where as the majority of the nodule shows less mineralization, having occurred with mineral to matrix ratio between 0.8 and 1.75. The mineralized nodules formed from the GF cell line also shows the highest mineralization occurring at the center with a mineral to matrix ratio of 3.5, while at the edges of the nodule no mineralization has occurred. The BCMP and SHED cell lines grew mineralized nodules with the highest mineral content of all the samples with mineral to matrix ratios of 5.0 and 5.2, respectively. However in the BCMP sample the most mineralized area occurred through out the center of the nodule and slowly decreased towards the edges. While the SHED nodule had points of lower mineralization in the center of the sample and like the previous samples the edges were less mineralized. Around the edges the BCMP and SHED samples had values of 3.3 and 1.3 respectively. The mineralized nodule formed from the SCAP sample had a mineral to matrix ratio with a high of 3.9 in the middle of the sample, and 2.5 throughout the rest of the mineralized area to the edges. The highest points of mineralization occurred towards the center in all of the cell lines, while lower values were found around the edges, probably due to the mineral in this area is still in the process of forming.

Further comparison of the mineralized nodules came from analysis of the carbonate to phosphate ratio. The maps for the carbonate to phosphate ratio are shown in figure 3.3.4. In the SHED nodule, the substrate peak's intensity was much greater than in the other samples, and the carbonate peak could not be observed. Most likely indicating the mineralized nodule grown was thinner than the rest of the samples. In the BCMP and GF cell lines the carbonate to phosphate ratio remained constant throughout the entire mineralized nodule. These cells lines gave values of 0.19 and 0.15 for the carbonate to phosphate ratio in the BMCP and GF cell lines, respectively. The mineralized nodules grown from the DPA, PDL and SCAP cell lines had values for the carbonate to phosphate ratio which varied depending on the location in the nodule. Higher values of the carbonate to phosphate ratio were observed around the edges, with values of 0.20, 0.17 and 0.13 for the DPA, PDL and SCAP nodules, respectively. In the center of the nodules a smaller value was observed for the carbonate to phosphate ratio. The DPA showed the greatest difference in the amount carbonate to phosphate ratio, with a value of 0.08 in the center of the nodule. The PDL and SCAP showed a smaller variation in the carbonate to phosphate ratio throughout the sample, and at their center had values of 0.13 and 0.10.

To examine the consistency of the mineral throughout the nodule an analysis of the 960 shoulder corresponding to an amorphous phosphate and the 960 peak corresponding to the crystalline component of the mineral was calculated. The maps of the ratio of amorphous phosphate to crystalline phosphate are seen in figure 3.3.5. In the BCMP and SCAP samples a consistent ratio of the amorphous phosphate to crystalline phosphate is observed across the entire nodule, with values of 0.24 and 0.3, respectively. The DPA, PDL and GF samples gave higher ratios around the edges and lower values in the center of the nodule. The DPA sample gave the largest variation with a ratio of 0.7 amorphous phosphate around the edges and 0.25 in the

center. In the PDL and GF samples a value of .5 was observed around the edges in both of the samples, while in the center the GF had a slightly lower component of amorphous phosphate with a ratio of 0.2 compared to 0.25 for the PDL. The nodules formed from the SHED cell line gave much a much lower value for the amorphous phosphate in the edge of the sample at 0.05 while in the center it had a much higher component than that seen in any of the previous samples with a ratio of 0.37.

Analysis of the area of the collagen peak over the mapping region can be seen in figure 3.3.6. The DPA sample shows three times more collagen present towards the edge of the sample, which is less mineralized. The other samples all show a correlation between the amount of collagen and the mineral. In the PDL, SCAP and BCMP samples there is four times as much collagen in the mineralized areas compared to the less mineralized areas. The GF samples show about 3 times as much collagen in the mineralized area when compared to the less mineralized area. The nodule from the SHED sample showed a pretty consistent amount of collagen throughout the whole sample, but there was a slight increase in the mineralized area, which had approximately 50% more collagen. To better quantify the amount of collagen present in the sample the ratio between the 960 phosphate peak and the collagen was calculated.

Raman mapping data can be seen in figure 3.3.7 for the ratio between the 960 phosphate peak and the collagen peak. For the SHED sample the ratio was found to be about 20 through out the entire sample. For the BCMP sample the mineral to collagen ratio was found to increase in the mineralized regions of the sample with values ranging between 40 to 65 compared to values of 20 to 30 around the edges. In the GF sample there was less variation, in the center of the sample there were points with higher mineral to collagen ratios ranging from 25 to 48, while around the edges of the sample the ratio ranged from 15 to 25. The DPA sample also showed a

smaller variation in the mineral to collagen ratio, which was about 25 in the area of high mineralization and between 10 to 15 in areas where less mineralization was present. In the PDL sample the mineralized nodules revealed ratios similar to the BCMP sample, with a mineral to collagen ratio of almost 50 in the center of the sample where the most mineralization had occurred and 15 to 25 around the edges. Lastly the SCAP sample had a lower mineral to collagen ratio in the higher mineralized areas with values in the range of 13 to 20, while around the edges the ratio was found to be between 17 and 27.

The residual stress in a sample leads to a shift in the Raman position of the peak, the mapping data from the Raman experiments can be seen in figure 3.3.8. The position of the 960 peak showed little variation throughout the mapping regions in the samples although there were some slight changes in the peak position in between the samples. In the GF and PDL samples, the position of the 960 peak was found to be 960.6 and 960.3 cm^{-1}, respectively, indicating no significant amount of stress between these samples. In the DPA, SCAP and SHED samples there the peak position averaged to be 958.4, 958.6 and 958.4 cm^{-1}, respectively, indicating similar amounts of stress in the mineral component in these samples. The BCMP nodules gave a peak position averaging to 959.0 cm^{-1}. The change in the 960 peaks position indicates a lower level of stress in the mineral in the GF and PDL samples and a higher amount of stress in the DPA, SCAP and SHED samples, leaving the BCMP sample in the middle.

Further analysis of the mineral component in the nodules included an analysis of the width of the v1 960 peak. The peaks width is used to determine the amount of order in the sample, the broader the peak is detected the less order there is in the crystal structure. The peak widths over the mapping region can be seen in figure 3.3.9. The SCAP and GF samples were both observed to have a peak width averaging to 15.91 cm^{-1}, with the PDL and BCMP sample

giving similar values calculated to be 15.83 and 15.97 cm^{-1} respectively. Indicating the

mineralized nodule has similar order in these structures. The DPA and SHED samples, were

found to have a larger peak width that averaged to 17.28 and 17.45 cm^{-1}, respectively. The shift

in the peak width in these samples suggest a significant amount of disorder in the crystal

structure of the nodules, when compared to the other 4 samples.

Analysis of the organic component of the mineralized nodules was conducted by

observing the width and position of the amide I peak. The data for the peak position of the

amide I peak can be seen in figure 3.3.9. In the PDL, DPA and SHED samples there was an

increase in the peak position toward the center of the nodule. The PDL and DPA samples

showed only a small change in the amide I position in the more mineralized areas and the SHED

sample showed a larger variation in the position. In the PDL sample the amide I peak was

observed around 1659 cm^{-1} in the less mineralized area, while in the mineralized area it was

observed at 1664 cm^{-1}. The DPA sample showed a similar change with the position observed at

1665 cm^{-1} in lower mineralized areas and 1670 cm^{-1} in the areas where more mineralization had

occurred. The SHED sample had the largest variation in peak position, which was observed at

1665 cm^{-1} in the lower mineralized areas and ranging from 1670 to 1680 cm^{-1} in areas where

more mineralization was apparent. The other samples showed a different relationship between

the peak position, having higher positions in the regions where less mineralization had occurred

and a smaller values in the areas where mineralization was more apparent. The BCMP sample

showed only a small shift in the peak position from 1667 to 1664 cm^{-1} between the lower and

higher mineralized areas, respectively. In the GF sample the more mineralized areas had values

around 1660 cm^{-1} where as the areas of lower mineralization had a peak position of 1664 cm^{-1}.

The SCAP sample had higher a higher peak position at 1670 cm^{-1}, in the areas of low

mineralization and a peak position of 1665 cm^{-1} in the areas of higher mineralization. The less mineralized areas are most likely where the mineralization is not yet complete and are observed predominantly around the edges of the sample. The observation of the peak positions moving towards lower positions in the BCMP, SCAP and GF samples and higher positions in the PDL, DPA and SHED samples indicates a change in the mineralization process between these samples. To further understand the difference in the organic component during mineralization analysis of the peak width of the amide I band was conducted.

The peak width of the amide I band throughout the Raman mapping region can be seen in figure 3.3.10. The change in the amide I peak width was observed to have a similar relationship as the position of the amide I peak. In the samples, which showed a decrease in the peak position between the high and low mineralized regions also, had a decrease in the peak position between these regions and the samples, in which an increase in the peak position was observed, also had an increase in the peak width, except in the PDL samples. The PDL sample had an amide I peak width at approximately 50 cm^{-1} in the areas of lower mineralization and a width of 46 cm^{-1} in the regions where more mineralization had occurred. The DPA and SHED samples were observed to have a decrease in the increase in peak width in the more mineralized area, with widths ranging from 68 to 80 cm^{-1} and 68 cm^{-1}, respectively. The BCMP, SCAP and GF nodules peak widths of 75, 56 and 65 cm^{-1}, were observed in areas of low mineralization and peak widths of 55, 45 and 50 cm^{-1} were observed in regions of higher mineralization, respectively. This suggests in the PDL, BCMP, SCAP and GF cell lines mineralization occurs with a less organized matrix prior to mineralization, and organic matrix with higher order after mineralization has completed. In the DPA and SHED cell lines it appears a more organized matrix is needed for mineralization that loses its order once mineralization has occurred.

36

Similar studies of biominerals formed by stem cells have been conducted using Raman microscopy, a recent study involving bone grown from stems cells of mouse embryonic stem cells, neonatal calvarial osteoblasts and mesenchymal stem cells, reported values for the mineral to matrix ratio, carbonate to phosphate ratio, and the position and width of the v1 phosphate peak.[9] While there are differences in the structure of bone and dentin, both materials have similar compositions and Raman spectra. The study found that mesenchymal stem cells and neonatal calvarial osteoblasts produced a mineral that closely resembled bone, and gave mineral to matrix ratios of 6.58 and 6.26, respectively, compared to 3.8 for native bone[9]. While the embryonic stem cells gave a material that was not consistent with bone and had a mineral to matrix ratio of 2.47. Comparing the biomineral grown from our dental stem cells to this study and our study of the mice teeth, it appears that the DPA stem cells grew a biomineral that was the least comparable to native dentin. The SHED and SCAP samples had a mineral to matrix ratio similar to that of native bone reported in by *Gentleman E*. The BCMP mineral to matrix ratio was closest to that of the neonatal calvarial osteoblasts and mesenchymal stem cells, which were reported to give a material most like that of native bone. Further comparison of the mineral to matrix ratio observed in the study of mice teeth, the PDL, GF and SHED samples gave a mineral to matrix ratio most comparable to the mice teeth. However when bone and dentin are formed naturally in vivo, there are mechanical forces which are suspected to influence the outcomes of the biomineral. The mineral to matrix ratio provides a good comparison of biominerals, other compositional comparisons must be made.

The carbonate to phosphate ratio of the bone nodules from *Gentleman E* reported a value of 0.16 for native bone and 0.22, 0.16 and 0.12 for embryonic stem cells, osteoblasts and mesenchymal stem cells, respectively. Compared to the results of from the mice and human

teeth these values are more consistent to that which was observed in the human teeth which gave a carbonate to phosphate ratio of 0.18 while the mice teeth were found to have a higher carbonate to phosphate ratio of 0.22. Again the DPA nodule was observed to produce a biomineral inconsistent of that of native dentin or bone. While the biomineral observed from the GF cell line gave a carbonate to phosphate ratio, similar to that observed in native bone and osteoblasts. The BCMP cell line was consistent with what was observed in human dentin. The SCAP and PDL mineralized nodules gave values lower than that observed in dentin, but consistent with what was observed in the mesenchymal stem cells. While the SCAP and PDL seem to form mineralized nodules similar to that of native biominerals, GF and BCMP appear to form the highest quality mineral, closest to that of dentin.

Analysis of the stress and order in the samples can be compared with the position and width of the v1 phosphate peak. Values for the position of the peak were reported to be 960.3, 960.3, 959.9 and 960.4 cm^{-1} by *Gentleman E* for native bone, embryonic stem cells and mesenchymal stem cells, respectively. These values were consistent with that observed in the mice teeth, which gave a position for the v1 phosphate peak of 960.4 cm^{-1}, however there was a large difference in the human teeth which gave a value of 962.8 cm^{-1}. The GF and PDL samples were observed to have similar levels of stress when compared to *Gentleman E*. and mice teeth. The nodule from the BCMP line was observed to have a slightly less amount of stress when compared to the peak position reported by *Gentleman E*. and mice teeth. The SHED, SCAP and DPA cell lines all gave positions of indicative of a lower amount of stress in the mineral component of the dentin. Analysis of the order of the crystalline hydroxyapatite, was also reported by *Gentleman E*, with values of 16.8, 16.5, 17.9 and 17.6 cm^{-1}, for native bone, embryonic stem cells and mesenchymal stem cells, respectively. When compared to the values

found in the mice teeth it appears the bone nodules had a significant amount of crystalline disorder, which gave widths in the 14.1 to 15.8 cm^{-1} range. The human teeth were observed to have an even more ordered crystalline component with a width of 12.0 cm^{-1} observed. The dental stem cell lines of PDL, BCMP, GF and SCAP all had values closest to that observed in the mice teeth, where as the DPA and SHED cell lines gave values closer to that of the osteoblasts and mesenchymal stem cells. However the role of mechanical forces in the biomineralization process in living tissues, could play a large role in the crystalline order and stress present in these samples.

While all the dental stem cell lines were able to produced mineralized nodules, it appears that the composition and material characteristics of these biominerals varied. When compared to Raman studies of other osseous materials and dentin from mice and humans, it appears that the GF and BCMP cell lines grow a mineral that is similar to that of dentin. While the other cell lines have some characteristics that are consistent with native dentin it appears that there are significant differences. A further study's of the mechanical properties of these nodules is needed, to accurately determine if these nodules have similar mechanical properties of dentin.

3.4 Hydroxyapatite samples

Hydroxyapatite coatings that were thermally sprayed were investigated by Raman spectroscopy. These samples are to be used in future experiments where osteoblasts will grown bone nodules on them. Before the biological experiment the Raman data was collected on the samples. The data from these samples can be seen in table 3.4. The full width at half max values is usually used to determine how much crystallinity the sample has; the sharp peaks of width 6.976 ± 0.05 indicate a high degree of crystallinity. Additionally there peak position was

observed at 963.544±0.038 cm^{-1} indicating a high amount of stress in the coatings compared to the normal value of hydroxyapatite at around 960 cm^{-1}. Finally the amount of amorphous phosphate to crystalline phosphate was determined to be 0.186±0.005. The mapping experiments showed the samples to be consistent in chemical composition throughout the area.

3.5 TiO2 Samples

After 14 days of culture, all TiO$_2$ samples had started to form deposits of collagen, nucleic acids and proteins. White light images can be seen in figure 3.5.1. The deposits were investigated by Raman spectroscopy. A characteristic spectrum from each mapping experiment is shown in figure 3.5.2. All scans were dominated by a peak at 1003 cm^{-1} which is characteristic of collagen. Other Raman peaks were observed at 1382 cm^{-1}, which is characteristic of nucleic acids and peaks at 1157 cm^{-1} which is indicative of a protein component. From previous studies on the mineralization in mice teeth collagen was observed to be an important factor in the early stages of mineralization, however as mineralization begins the collagen concentration is reduced and amino acids of proteins concentrations increase, especially phenylalanine. An analysis a ratio of the amount of collagen to the amount of protein determined by the area under the 1003 cm^{-1} peak and 1157 cm^{-1} peak was performed. Table 3.5 shows the calculated values of this ratio over the deposits.

It can be seen that the heat-treated sample at 300 °C, had the lowest amount of collagen with respect to proteins in all of the samples studied. Followed by 200 °C, 400 °C, as-received and finally 600 °C.   The increase in the amount of proteins available is indicative of better cell adhesion in this sample. The faster cells adhere and begin formation of the extra cellular matrix the quicker the mineralization process will be. Once the collagen scaffold is complete proteins

and other organic components are responsible for the growth of the hydroxyapatite crystal. Previous studies on these samples, indicated the 300 °C heat treated sample, had the highest concentrations of alkaline phosphatase an enzyme responsible for the removal of phosphate groups from nucleotides, proteins and alkaloids. Freeing phosphate groups are an important step in the mineralization process as phosphate is the main ion in the hydroxyapatite matrix. Further investigation of these deposits included the peak position and width of the collagen component.

The data for the peak width and position is also shown in table 3.5. The collagen appears to have a similar structure in all of the samples. The width of the collagen peak in the 300 °C heat-treated sample however shows a slight increase although it is with the 95% confidence limits of the other samples. The 95% confidence limit for this sample is much greater than the others indicating a larger variation in the calculated peak widths in this sample. This could be an indication that the collagen in the 300 °C heat-treated sample is in a more disordered state suggesting the collagen could be leaving its ordered scaffold. The peak position of the collagen appeared consistent throughout all the samples, a slight increase in the position was observed in the 200 °C heat-treated sample but only a 0.4 cm^{-1} shift and insignificant.

From the initial biological tests and Raman experiments it appears that the 300C heat treatment was the most successful it initiating an early biological response from osteoblasts. However a full 28-day cell culture is needed to determine if there are any differences in the fully mineralized nodules between the samples and native bone

4.0 Conclusion

The process of mineralization is an important biological phenomenon that needs further understanding in order to engineer devices to optimize this response. Raman spectroscopy is a useful tool to provide insight into this phenomenon because of its ability to characterize both the organic and inorganic components of these materials without destructive sample preparation techniques.

Observations of irregular dentin in mice teeth provided insight on how dentin forms and the important biological components, which aid in the mineralization process. In areas of irregular dentin, collagen and phenylalanine where found in increased concentrations. The collagen was observed to play a role in the earlier stages of mineralization, where there where low mineral to matrix ratios. As the dentin matured phenylalanine was observed in greater concentrations followed by a reduction in the amount of collagen.

Biologists and biological engineers have discovered various stem cells, which can produce biomineralized deposits. Traditional biological tests lack the insight to the material characteristics to compare these biological materials to native tissues. By using a material based spectroscopic approach, Raman spectroscopy was able to identify the compositions of this mineralized deposits a provide greater insight into the mineral and organic structures. Stem cells from DPA and SHED were found to produce mineralized deposits, which significantly differed in crystalline structure and composition from native dentin, while the BCMP and GF cell lines produced a much higher quality dentin like substance.

While advancements have been made in endoprosthetic implants, most of these advancements come in the form of changing the microscopic properties of a material to illicit a specific biological response. While these relationships are important few new materials have

made it into these devices. Early work done on titanium dioxide has revealed its enormous

potential as a new material for implants. The investigation of various heat-treated TiO_2

substrates cultured with osteoblasts, have shown it potential to as a new biomaterial. As well as

provide information on the relationship between the surface free energy of a material and the

biological response it will induce.

The results from these experiments show the enormous potential in the viability of

Raman spectroscopy for characterization of mineralized biological tissues, as well as its ability to

characterize the microstructure and compositions of materials for endoprosthetic implants.

5.0 Future Work

A further comparison of the nodules from the dentin stem cells in needed in order to determine how their mechanical behavior compares to that of native dentin. By using nanoindentation we can determine the stiffness of the nodules to provide a better comparison between native dentin and these nodules.

The thermally sprayed hydroxyapatite coatings will be heat treated and cultured at 28 days using osteoblasts. The mineral formed on these substrates will be investigated by Raman spectroscopy to determine any differences in the minerals composition, and to observe how hydroxyapatite coatings become incorporated into regenerating bone. A similar study will be carried out on the titania heat-treated substrates, with a full 28 day study so the nodules become mineralized. To determine if the composition of the mineral produced on the different heat treated substrates is the same as native bone.

References

1   Meirelles, L. *et al.* Effect of Hydroxyapatite and Titania Nanostructures on Early In Vivo Bone Response. *Clinical Implant Dentistry and Related Research* **10**, 245-254, doi:10.1111/j.1708-8208.2008.00089.x (2008).

2   Lowenstam, H. A. MINERALS FORMED BY ORGANISMS. *Science* **211**, 1126-1131, doi:10.1126/science.7008198 (1981).

3   Carden, A. & Morris, M. D. Application of vibrational spectroscopy to the study of mineralized tissues (review). *Journal of Biomedical Optics* **5**, 259-268, doi:10.1117/1.429994 (2000).

4   Movasaghi, Z., Rehman, S. & Rehman, I. U. Raman spectroscopy of biological tissues. *Applied Spectroscopy Reviews* **42**, 493-541, doi:10.1080/05704920701551530 (2007).

5   Rho, J. Y., Kuhn-Spearing, L. & Zioupos, P. Mechanical properties and the hierarchical structure of bone. *Medical Engineering & Physics* **20**, 92-102, doi:10.1016/s1350-4533(98)00007-1 (1998).

6   PG, R. Vertebrate mineralized matrix proteins: Structure and function. . *Calcif Tissue Res* **25**, 169-178 (1996).

7   Ito A, O. K. in *Crystal Growth Technology*   (ed Tadashi Ohachi K. Byrappa) Ch. 16, 525-558 (2003).

8   O. Akkus, F. A., M.B Schaffler. Age-related changes in physicochemical properties of mineral crystals are related to impared mechanical function of cortical bone. *Bone* **34**, 443 (2004).

9   Gentleman, E. *et al.* Comparative materials differences revealed in engineered bone as a function of cell-specific differentiation. *Nature Materials* **8**, 763-770, doi:10.1038/nmat2505 (2009).

10   Marshall, G. W., Marshall, S. J., Kinney, J. H. & Balooch, M. The dentin substrate: structure and properties related to bonding. *Journal of Dentistry* **25**, 441-458, doi:10.1016/s0300-5712(96)00065-6 (1997).

11   Dusevich, V., Xu, C. Q., Wang, Y., Walker, M. P. & Gorski, J. P. Identification of a protein-containing enamel matrix layer which bridges with the dentine-enamel junction of adult human teeth. *Archives of Oral Biology* **57**, 1585-1594, doi:10.1016/j.archoralbio.2012.04.014 (2012).

12   Elliot, J. *Structure and chemistry of apatites and other calcium orthophosphates*. (1994).

13   Posner AS, S. J., Lippincott ER. Hyrdogen-bonding in calcium-deficient hydroxyapatite. *Nature* **188**, 486-487 (1960).

14   Midy, V., Rey, C., Bres, E. & Dard, M. Basic fibroblast growth factor adsorption and release properties of calcium phosphate. *Journal of Biomedical Materials Research* **41**, 405-411, doi:10.1002/(sici)1097-4636(19980905)41:3<405::aid-jbm10>3.0.co;2-h (1998).

15   Heimann, R. B. Thermal spraying of biomaterials. *Surface & Coatings Technology* **201**, 2012-2019, doi:10.1016/j.surfcoat.2006.04.052 (2006).

16   Miller, B. F. K., Claire B. *Encyclopedia and dictionary of medicine, nursing, and allied health.*, (1992).

17   Burg, K. J. L., Porter, S. & Kellam, J. F. Biomaterial developments for bone tissue engineering. *Biomaterials* **21**, 2347-2359, doi:10.1016/s0142-9612(00)00102-2 (2000).

18   Hench, L. L. BIOCERAMICS - FROM CONCEPT TO CLINIC. *Journal of the American Ceramic Society* **74**, 1487-1510, doi:10.1111/j.1151-2916.1991.tb07132.x (1991).

19   Gadow, R., Killinger, A. & Stiegler, N. Hydroxyapatite coatings for biomedical applications deposited by different thermal spray techniques. *Surface & Coatings Technology* **205**, 1157-1164, doi:10.1016/j.surfcoat.2010.03.059 (2010).

20   Batta, V. *et al.* Uncemented, custom-made, hydroxyapatite-coated collared distal femoral endoprostheses. *Bone & Joint Journal* **96B**, 263-269 (2014).

21   Unwin, P. S. *et al.* Aseptic loosening in cemented custom-made prosthetic replacements for bone tumours of the lower limb. *Journal of Bone and Joint Surgery-British Volume* **78B**, 5-13 (1996).

22   Cristofolini, L., Bini, S. & Toni, A. In vitro testing of a novel limb salvage prosthesis for the distal femur. *Clinical Biomechanics* **13**, 608-615, doi:10.1016/s0268-0033(98)00024-2 (1998).

23   Penel, G., Leroy, G., Rey, C. & Bres, E. MicroRaman spectral study of the PO4 and CO3 vibrational modes in synthetic and biological apatites. *Calcified Tissue International* **63**, 475-481, doi:10.1007/s002239900561 (1998).

24   Ducheyne, P., Radin, S. & King, L. THE EFFECT OF CALCIUM-PHOSPHATE CERAMIC COMPOSITION AND STRUCTURE ON INVITRO BEHAVIOR .1. DISSOLUTION. *Journal of Biomedical Materials Research* **27**, 25-34, doi:10.1002/jbm.820270105 (1993).

25   Boyan, B. D., Hummert, T. W., Dean, D. D. & Schwartz, Z. Role of material surfaces in regulating bone and cartilage cell response. *Biomaterials* **17**, 137-146, doi:10.1016/0142-9612(96)85758-9 (1996).

26   Swami, N., Cui, Z. W. & Nair, L. S. Titania Nanotubes: Novel Nanostructures for Improved Osseointegration. *Journal of Heat Transfer-Transactions of the Asme* **133**, 7, doi:10.1115/1.4002465 (2011).

27   Smith, E. D., G.   (ed John Wiley) (2005).

28   Ferraro, J. R., Nakamoto K., Brown C.W.,. *Introductoy Raman Spectroscopy*. (2003).

29   W.H., W. & R., M. *Raman Scattering in Materials Science*. (2000).

30   Manoharan, R., Wang, Y. & Feld, M. S. Histochemical analysis of biological tissues using Raman spectroscopy. *Spectrochimica Acta Part a-Molecular and Biomolecular Spectroscopy* **52**, 215-249, doi:10.1016/0584-8539(95)01573-6 (1996).

31   Xu, C. & Wang, Y. Chemical composition and structure of peritubular and intertubular human dentine revisited. *Archives of Oral Biology* **57**, 383-391, doi:10.1016/j.archoralbio.2011.09.008 (2012).

32   Weidner, T. *et al.* Direct Observation of Phenylalanine Orientations in Statherin Bound to Hydroxyapatite Surfaces. *Journal of the American Chemical Society* **134**, 8750-8753, doi:10.1021/ja301711w (2012).

Appendix
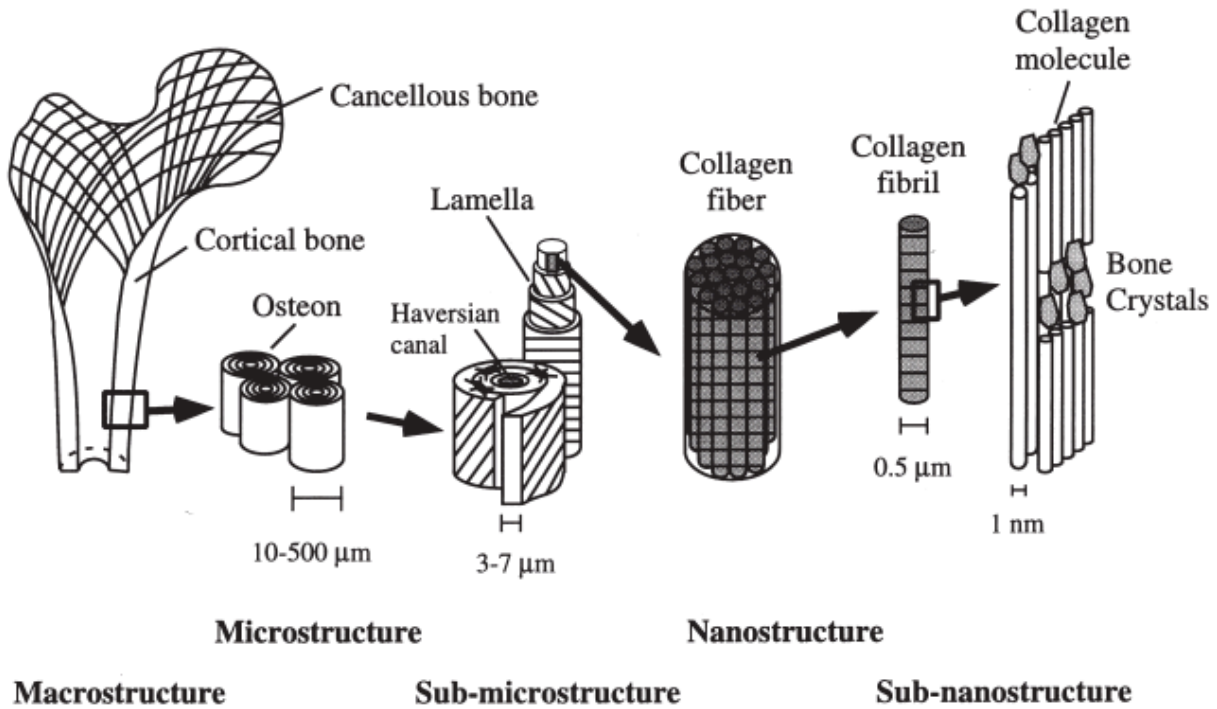
Figure 1.1.1. The hierarchal structure of bone at five different lengths. At the smallest scale hydroxyapatite crystals are wrapped in collagen to form sheets. These sheets wrap up to form fibrils.[5]
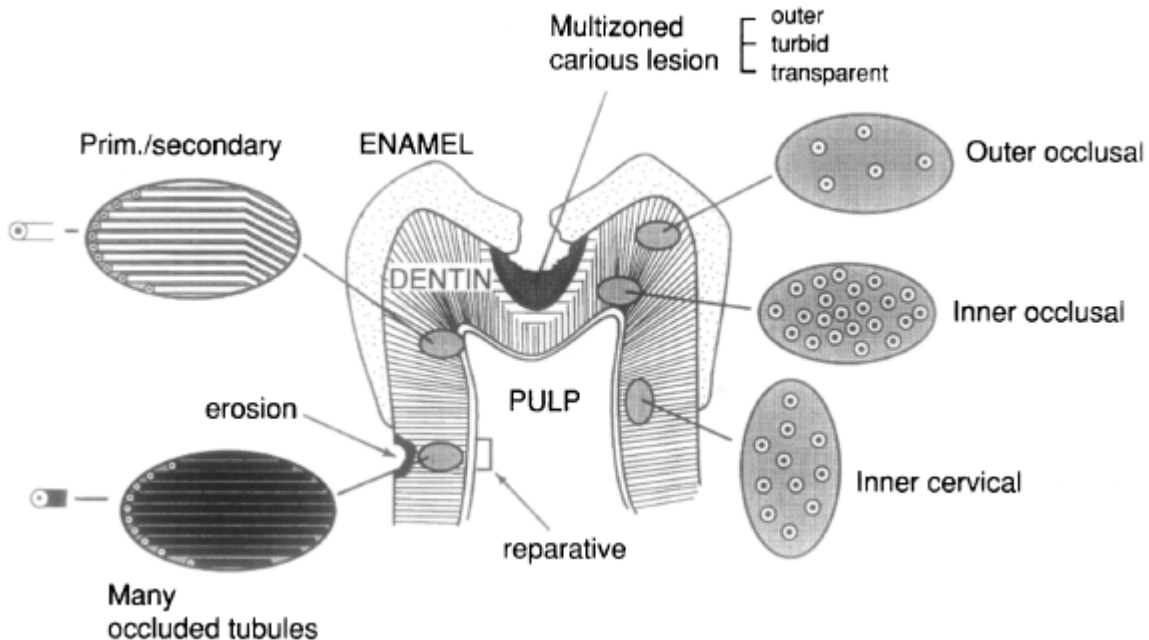
Figure 1.1.2. The structure of a tooth. The dentin surrounds the dental pulp chamber where odontoblastic cells are held supporting the odontoblastic processes in the dentin. Also shown are the tubules used by the odontoblastic cells for travel.[7]
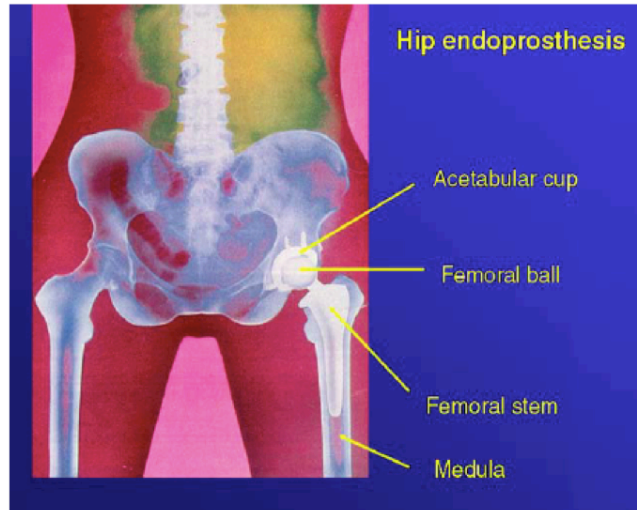
Figure 1.2.1. A typical hip implant. The femoral stem is drilled and mounted into the Medula, good fixation of the femoral stem to the medulla is essential to the implants survival.[12]
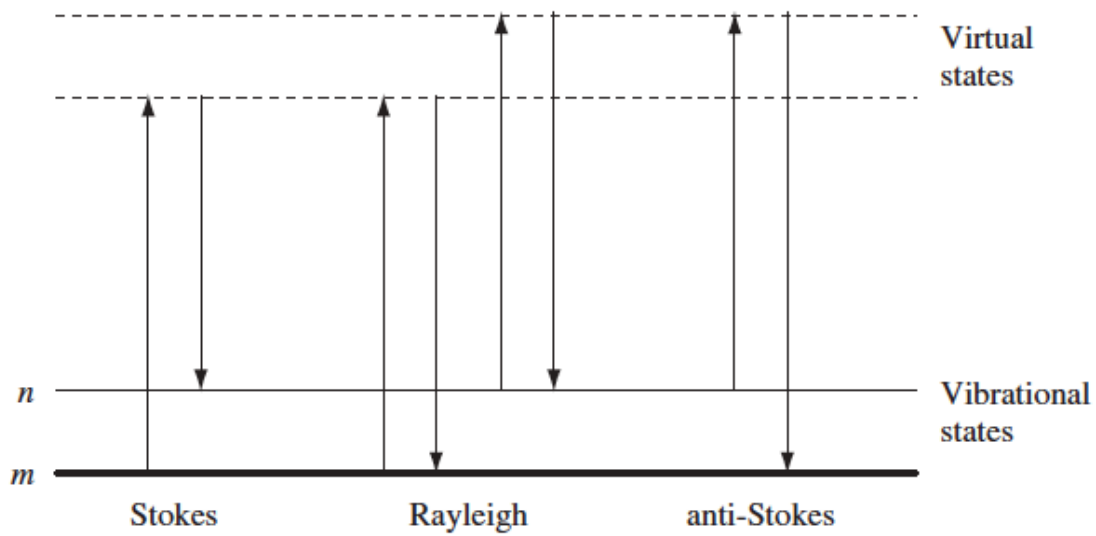
Figure 1.5.1. The scattering possibilities related to Raman. Rayleigh scattering is an elastic process where the energy of the system and photon remain the same. Where as in stokes and anti-stokes scattering energy is lost or gained in the scattering process, providing information on the bonds and crystal structure of the system.[27]
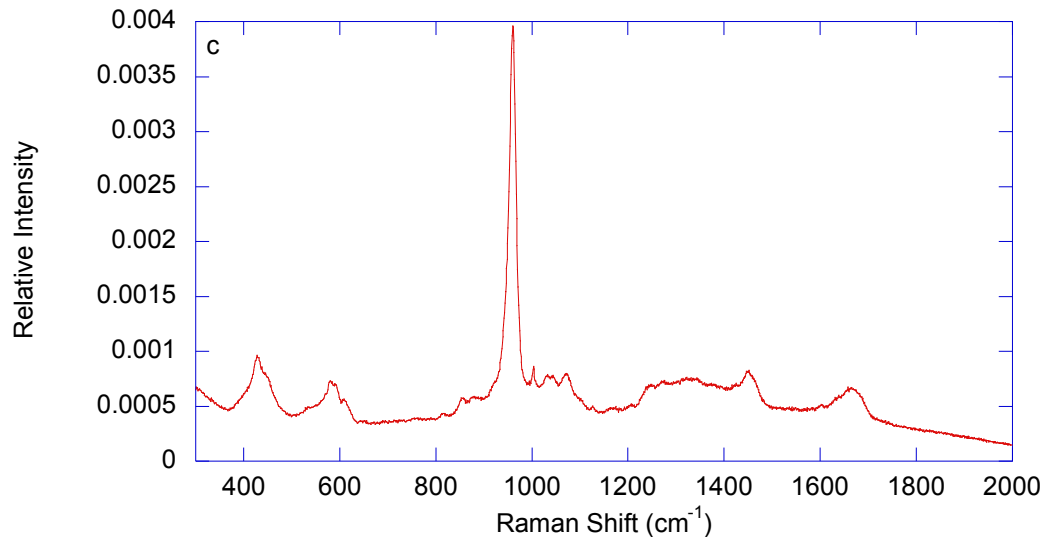
Figure 1.6.1. A characteristic Raman spectra of dentin. The v1, v2 and v4 phosphate peak can be seen at 960 cm^{-1}, 441cm^{-1} and 580 cm^{-1}. The carbonate substitution peak is also present at 1070 cm^{-1} and the collagen peak is observed at 1003 cm^{-1}. The broad peaks at, 1250 cm^{-1}, 1450 cm^{-1} and 1660 cm^{-1}, are characteristic of the organic components of the amide III envelope, CH$_2$ wag and the amide I mode. Also visible are peaks corresponding to phenylalanine at 651 cm^{-1}, 1579 cm^{-1} and 1601 cm^{-1}.
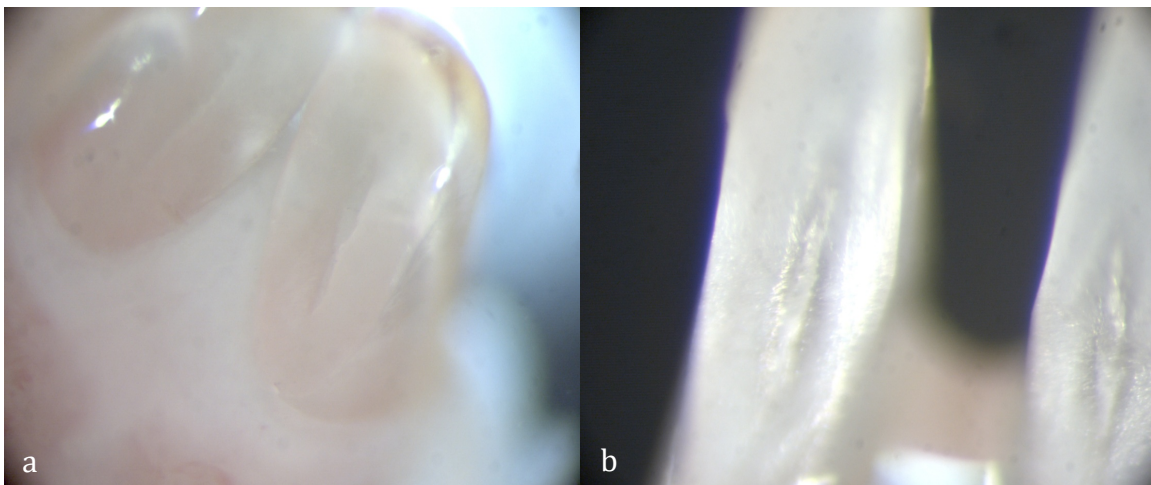
Figure 2.1.1. Images of the back side of mice teeth. The areas of irregular dentin can be seen as the white stripes going down the tooth. The lower incisor (**a**) and the (**b**) upper incisor both appeared to have these areas.
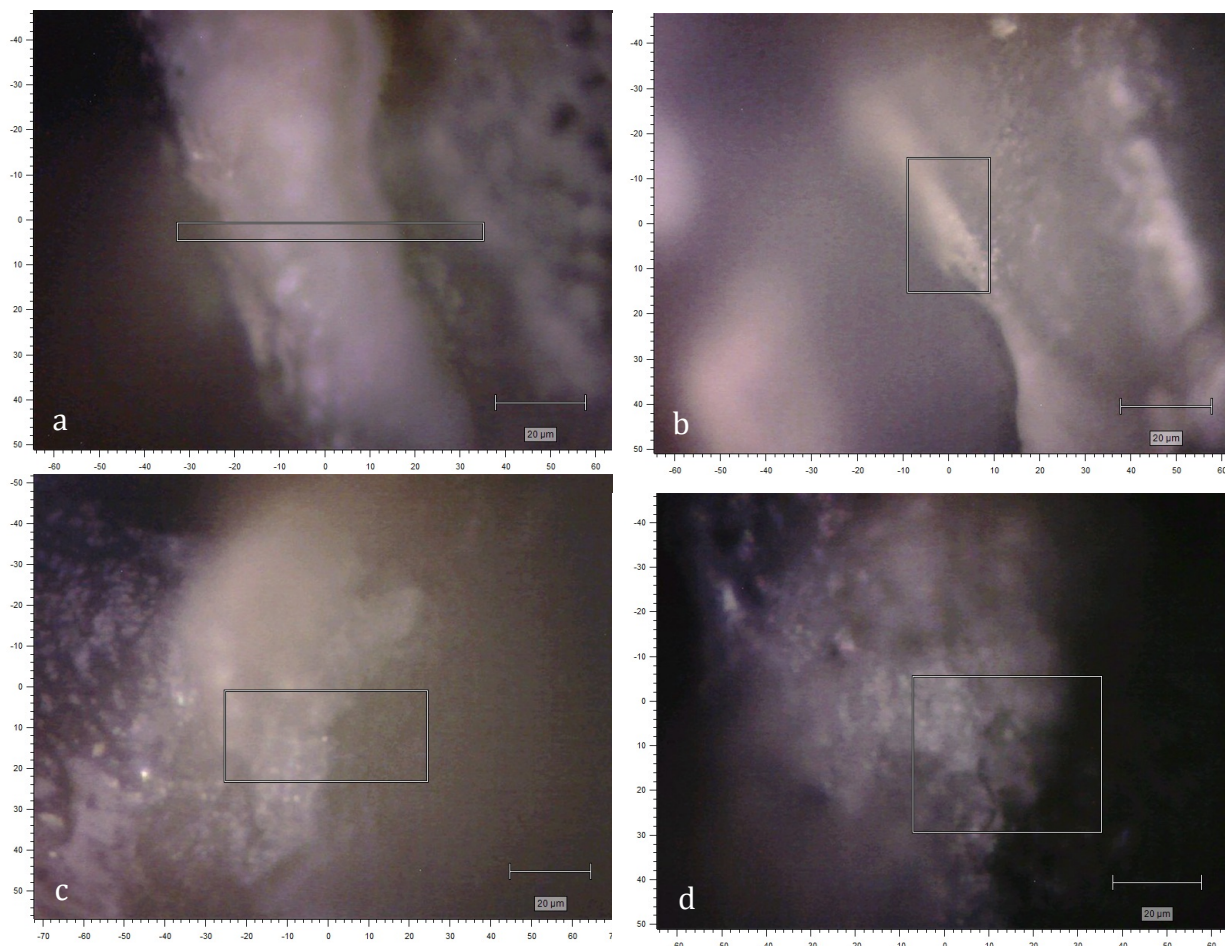
Figure 3.1.1. White light images of mice teeth over the areas of irregular dentin at 50x magnification. The areas in the box are the regions over which the Raman mapped. For (**a**) the upper incisor near the tip, (**b**) the upper incisor way from the tip, (**c**) the lower incisor near the tip and (**d**) the lower incisor away from the tip.
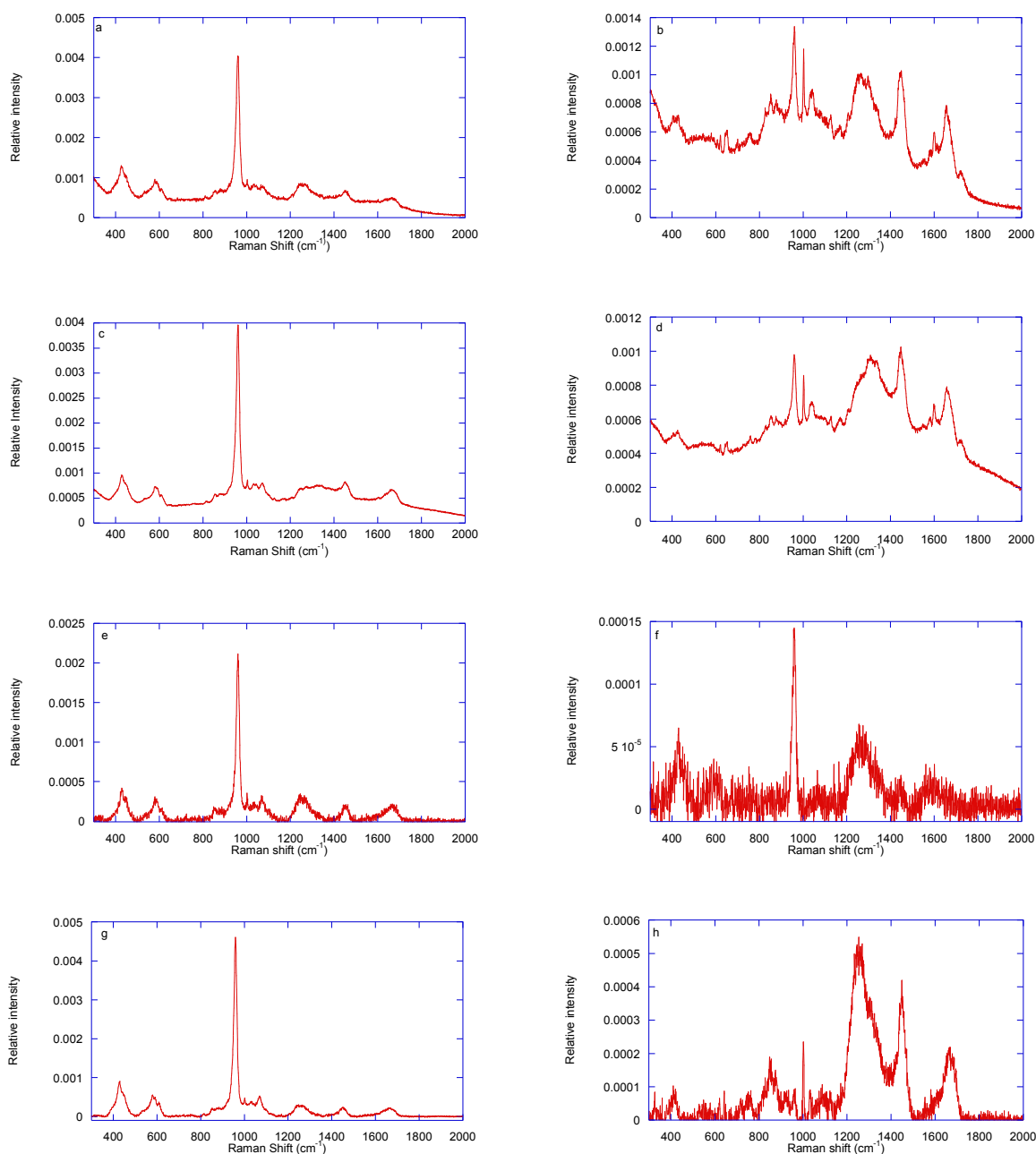
Figure 3.1.2. Characteristic Raman spectra of the mice teeth in the 300 to 2000 cm^{-1} region. Spectra from the areas of regular and irregular dentin are shown. Spectra from the mineralized areas (**a**, **c**, **e**, **g**) are dominated by the v1 phosphate band (960 cm^{-1}) characteristic of Hydroxyapatite, while spectra from the areas of irregular dentin (**b**, **d**, **f**, **h**) are influenced by the organic components such as the amide I band (~1660 cm^{-1}). **a-b** upper incisor near the tip of the tooth, **c-d** upper incisor away from the tooth, **e-f** lower incisor near the tip of the tooth, **g-h** lower incisor away from the tip.
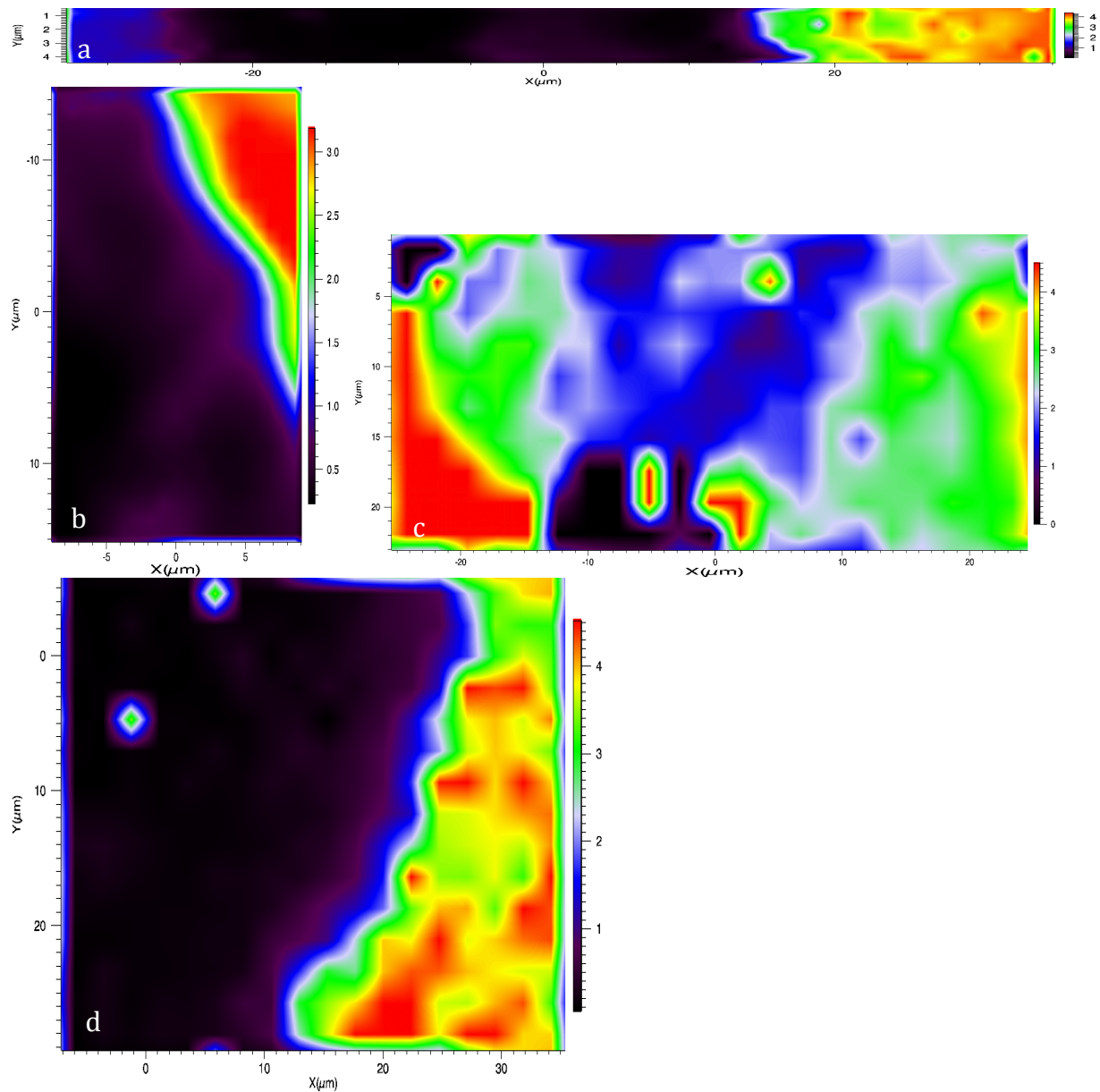
Figure 3.1.3. Mineral to matrix ratio calculated by the area under the v1 phosphate peak divided by the area of the amide I peak. For (**a**) the upper incisor near the tip, (**b**) the upper incisor way from the tip, (**c**) the lower incisor near the tip and (**d**) the lower incisor away from the tip.
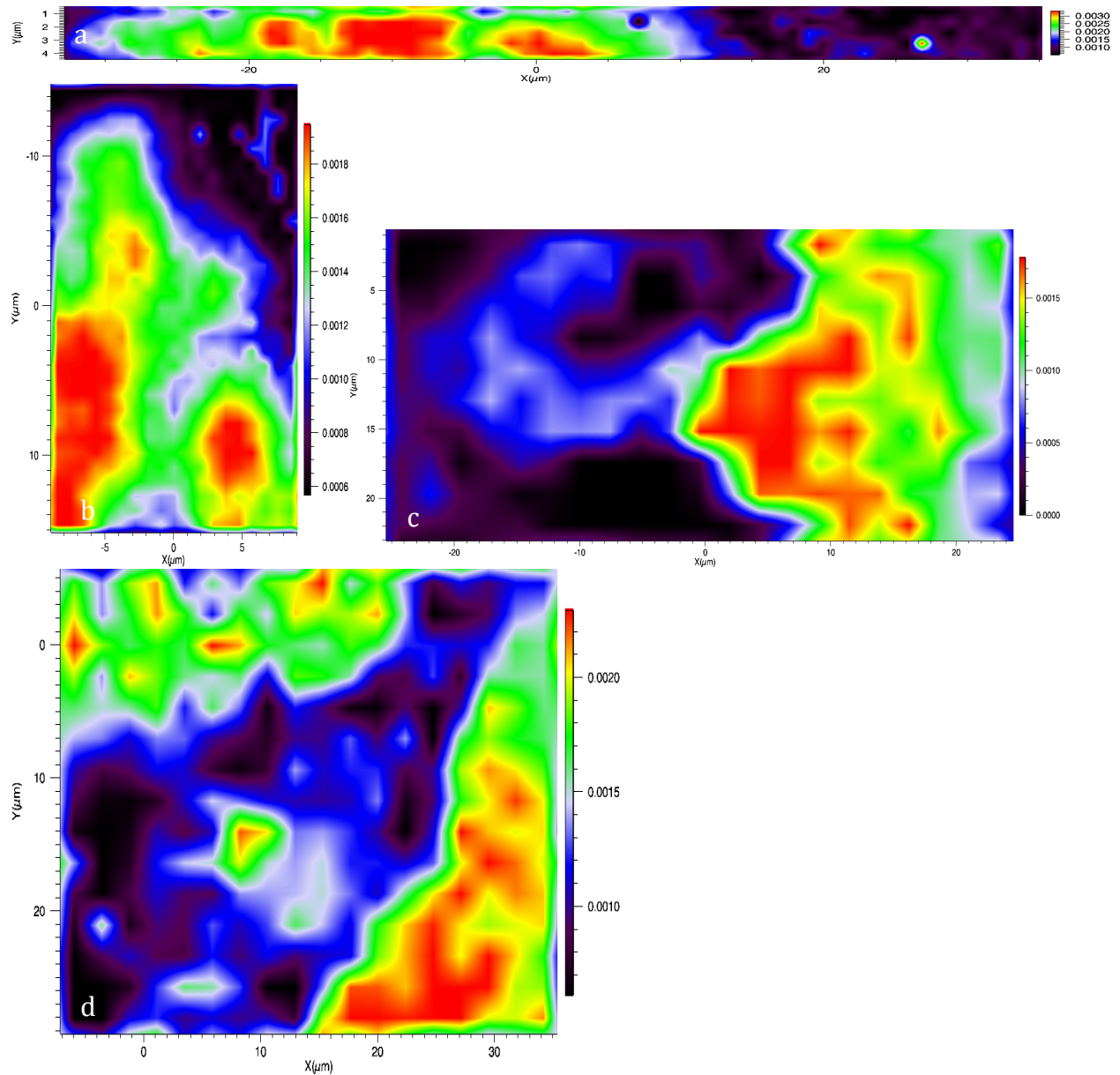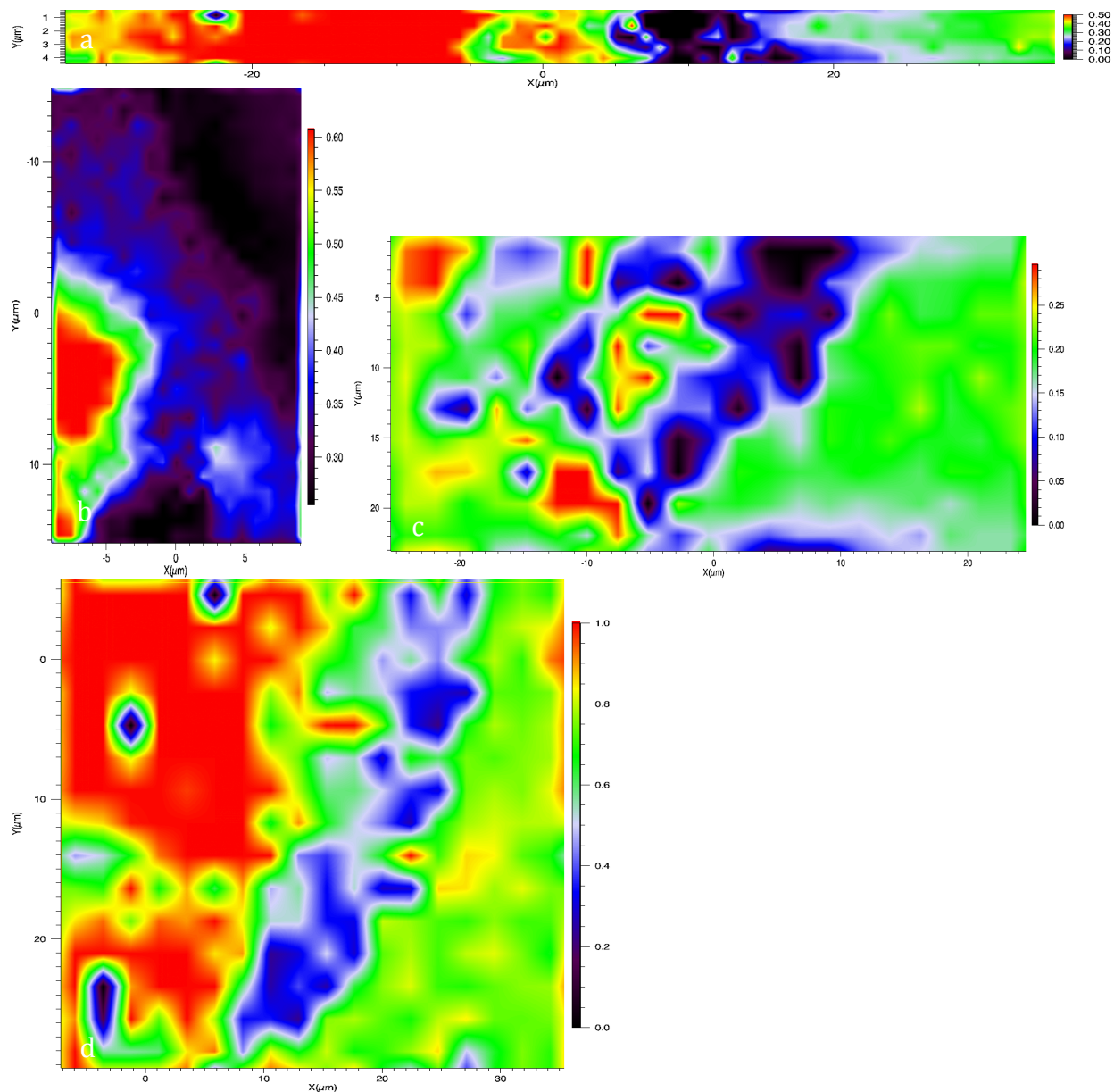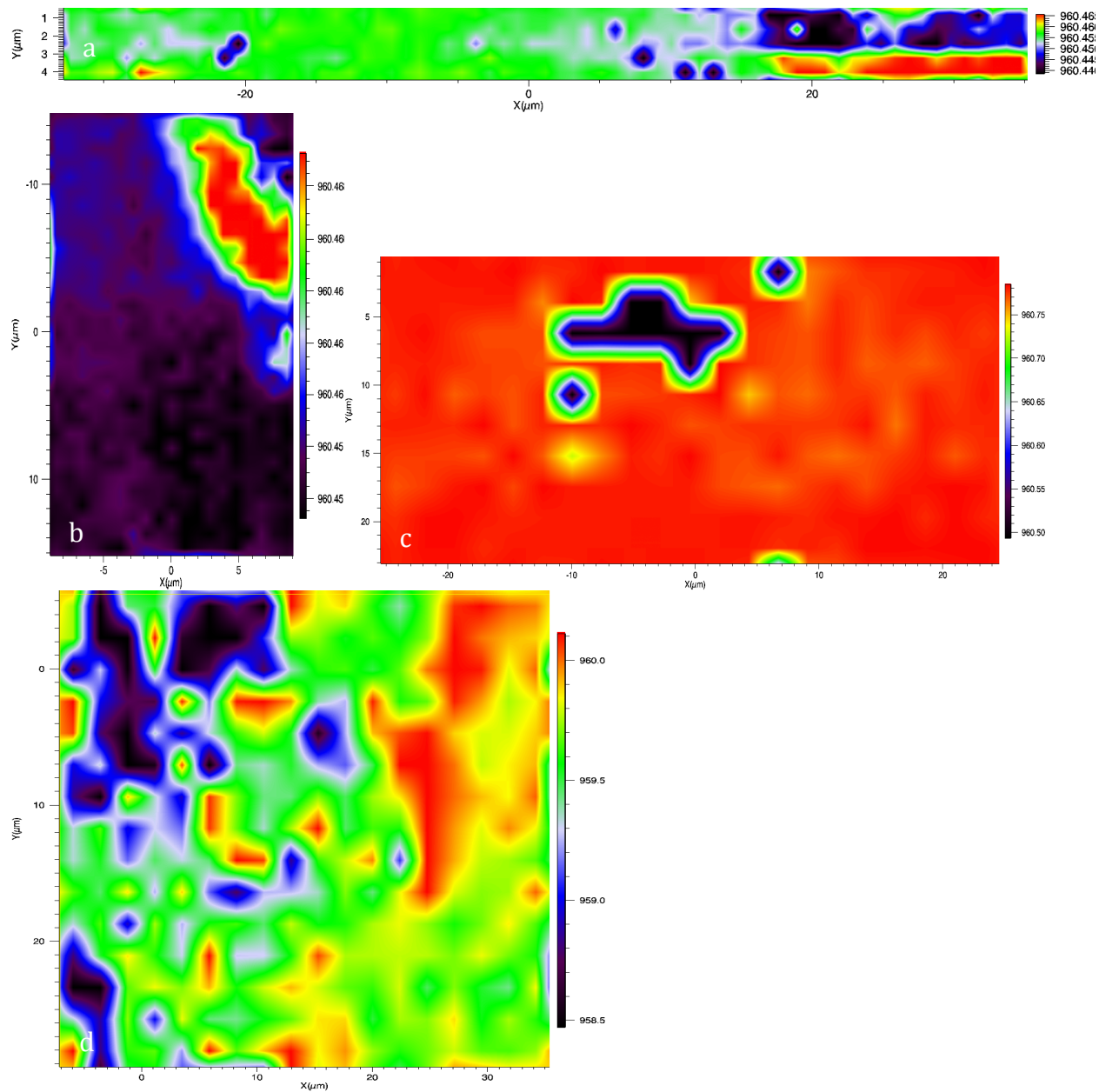
Figure 3.1.4. The area under the collagen curve plotted as a function of position. For (**a**) the upper incisor near the tip, (**b**) the upper incisor way from the tip, (**c**) the lower incisor near the tip and (**d**) the lower incisor away from the tip.
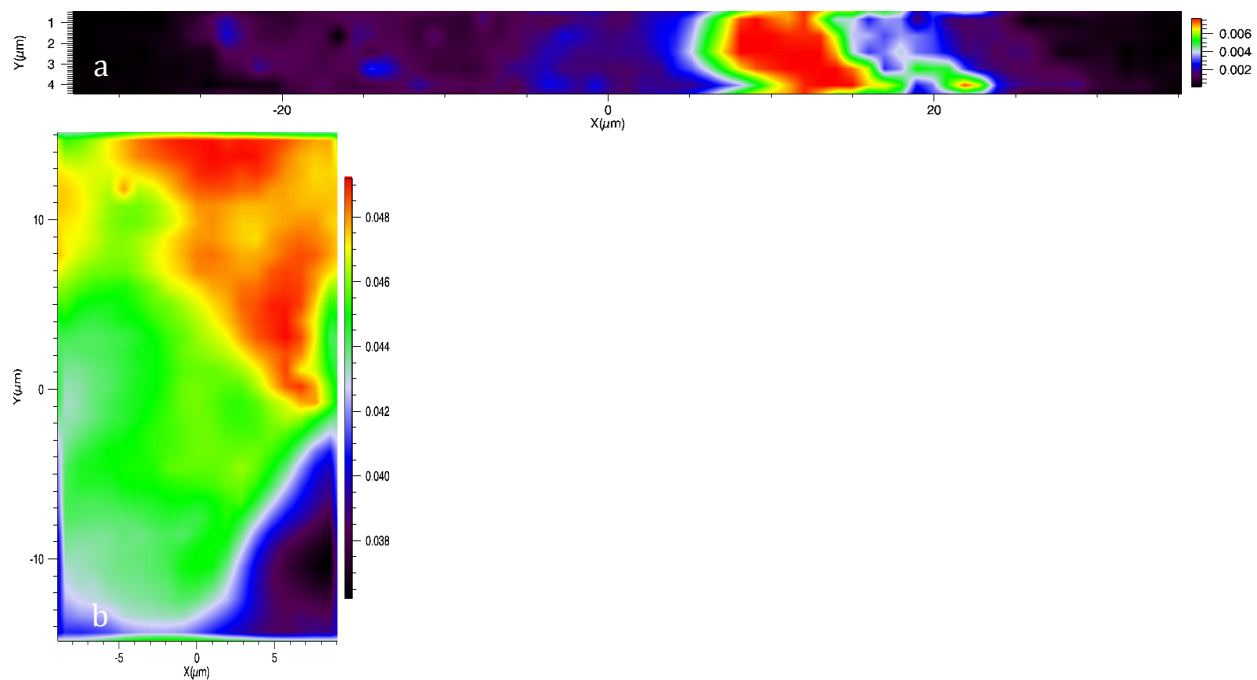
Figure 3.1.5. The area under the phenylalanine curve plotted as a function of position. For (**a**) the upper incisor near the tip and (**b**) the upper incisor way from the tip. Phenylalanine was not detected in either of the lower incisor spectra.
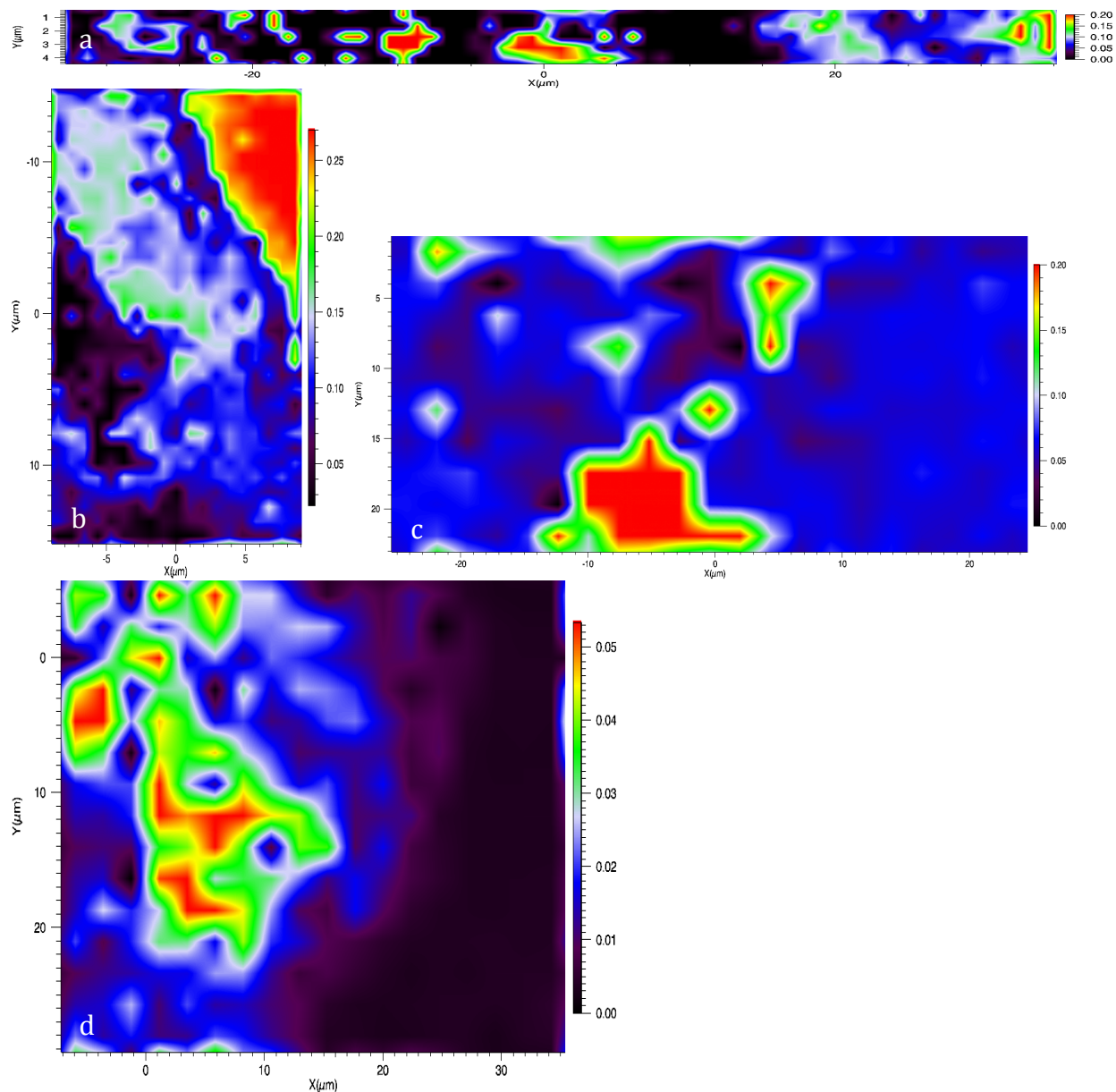
Figure 3.1.6. Carbonate to phosphate ratio calculated by the area under the 1070 cm^{-1} carbonate peak divided by the area of the v1 phosphate peak. For (**a**) the upper incisor near the tip, (**b**) the upper incisor way from the tip, (**c**) the lower incisor near the tip and (**d**) the lower incisor away from the tip.

Figure 3.1.7. Amorphous Phosphate to Crystalline Phosphate phosphate ratio calculated by the area under the 950 cm^{-1} amorphous phosphate peak divided by the area of the v1 phosphate peak. For (**a**) the upper incisor near the tip, (**b**) the upper incisor way from the tip, (**c**) the lower incisor near the tip and (**d**) the lower incisor away from the tip.
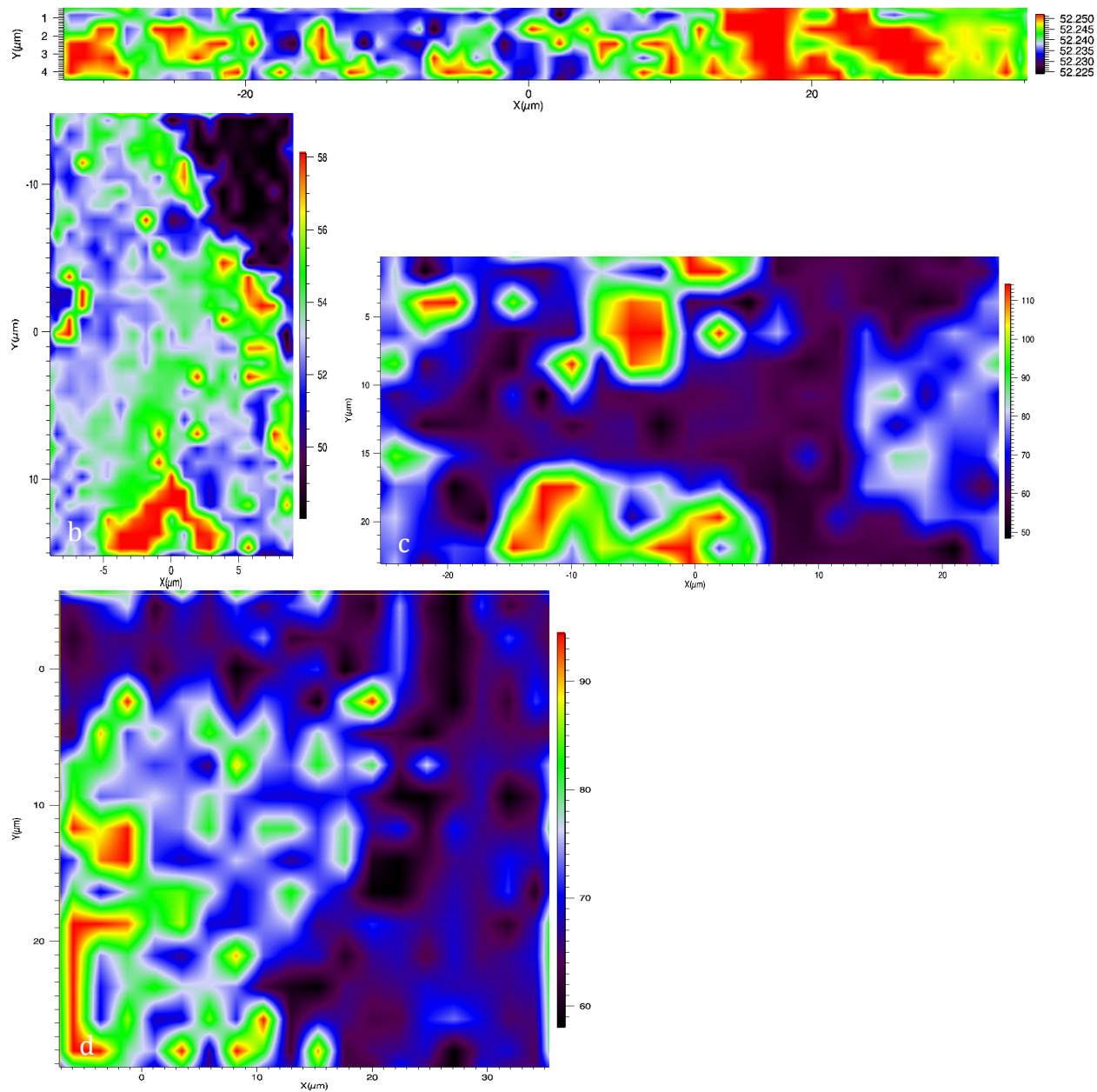
Figure 3.1.8. Position of the v_1 Phosphate peak for (**a**) the upper incisor near the tip, (**b**) the upper incisor way from the tip, (**c**)the lower incisor near the tip and (**d**) the lower incisor away from the tip.
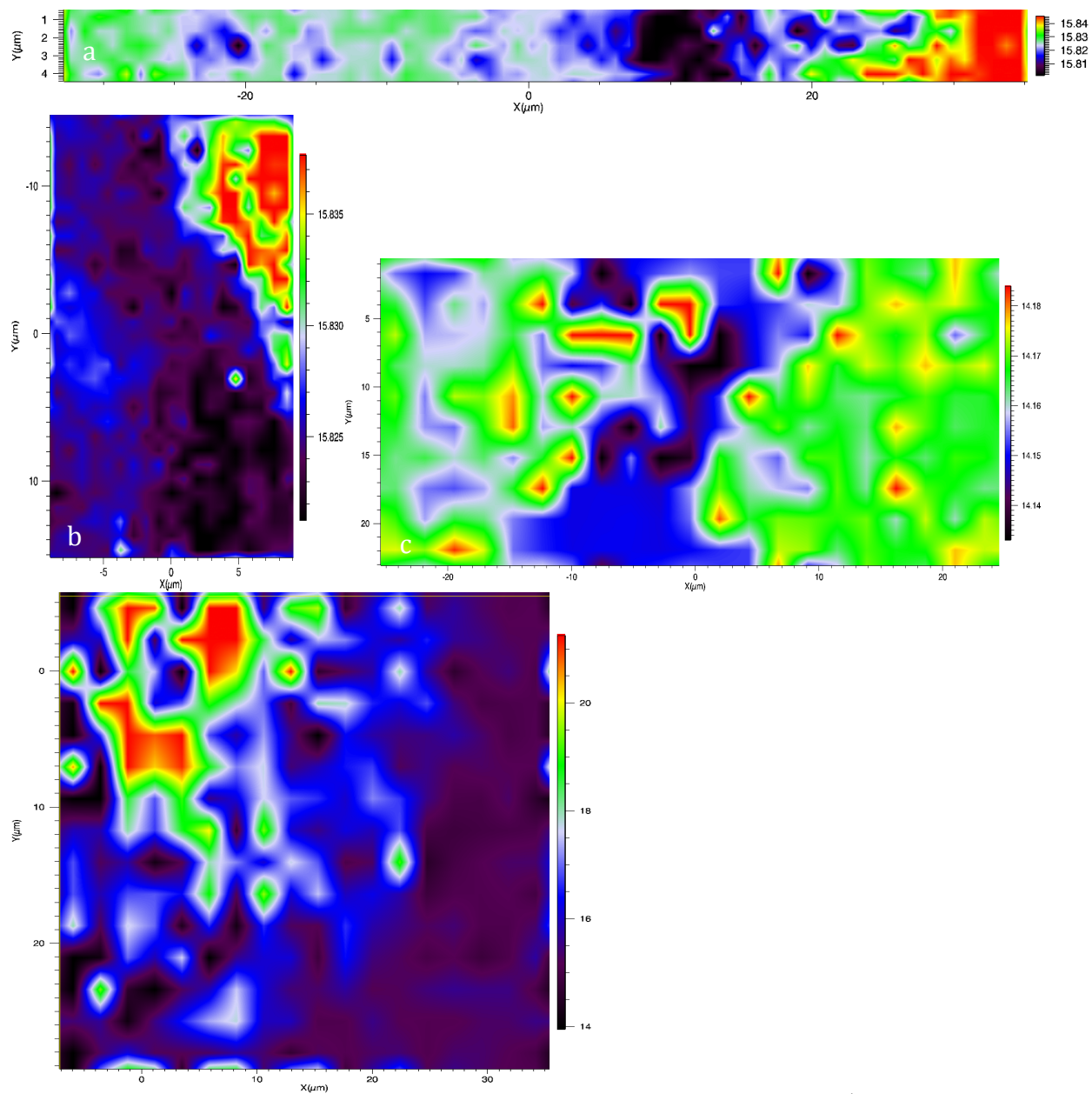
Figure 3.1.9. The full width at half max of the v1 phosphate peak (960 cm^{-1}) for (**a**) the upper incisor near the tip, (**b**) the upper incisor way from the tip, (**c**)the lower incisor near the tip and (**d**) the lower incisor away from the tip.
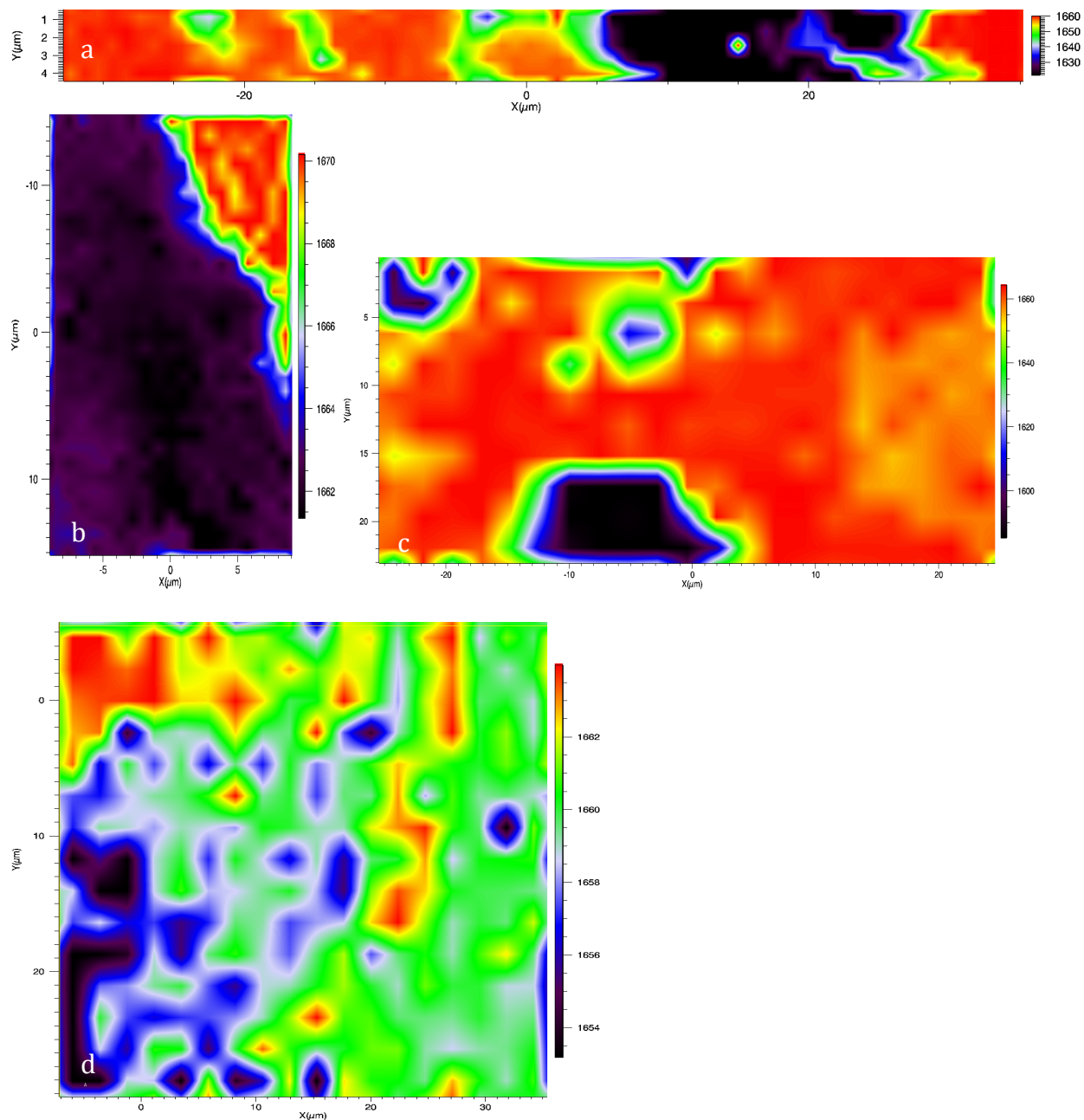
Figure 3.1.10. The peak position of the amide I band for (**a**) the upper incisor near the tip, (**b**) the upper incisor way from the tip, (**c**) the lower incisor near the tip and (**d**) the lower incisor away from the tip.

Figure 3.1.11. The width is of the amide I band for (**a**) the upper incisor near the tip, (**b**) the upper incisor way from the tip, (**c**) the lower incisor near the tip and (**d**) the lower incisor away from the tip.
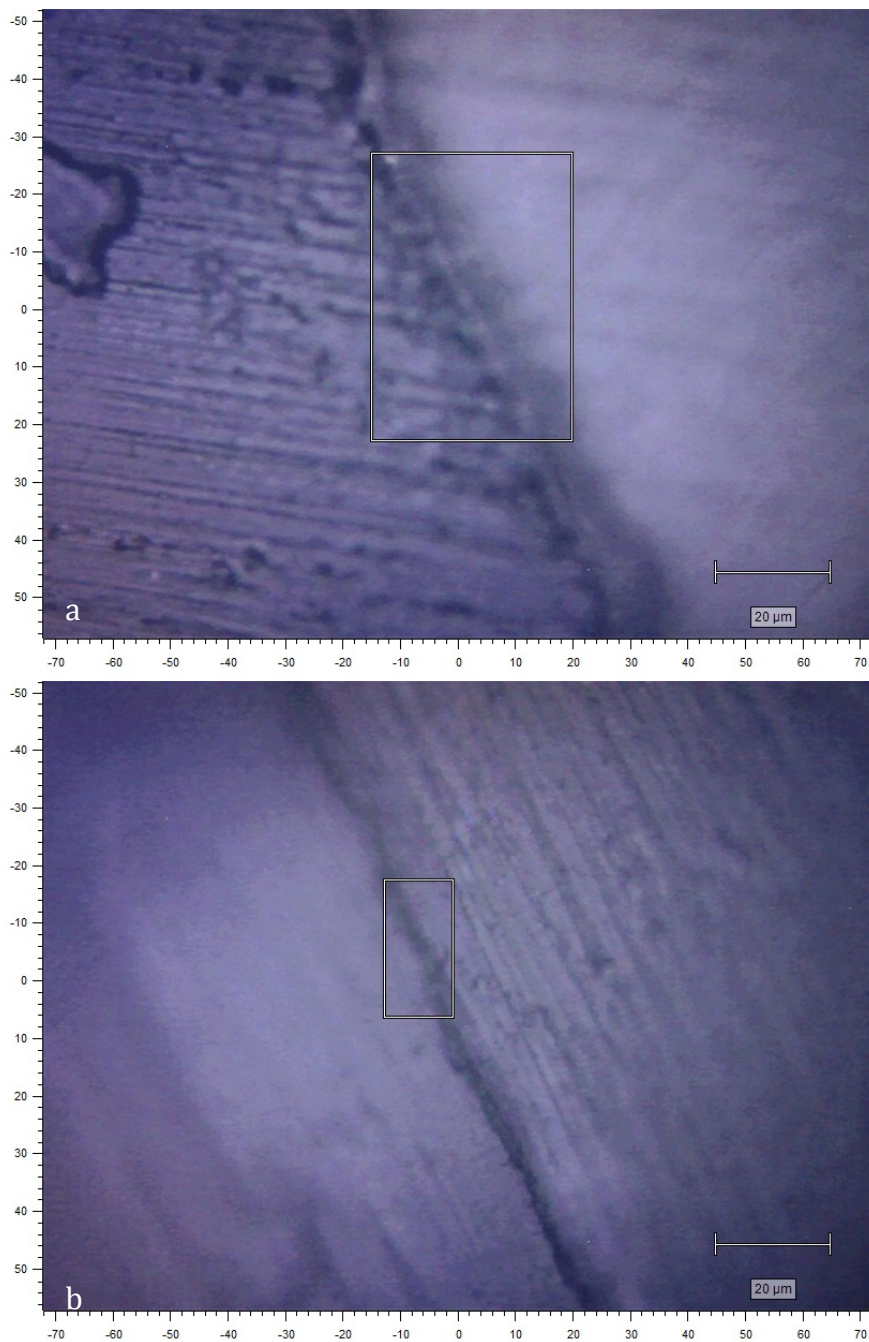
Figure 3.2.1. White light images of the adult and deciduous teeth near the dental-enamel junction at 50x magnification after polishing.   The Raman mapping area is indicated by the box. (a) The adult tooth, (b) the deciduous tooth.
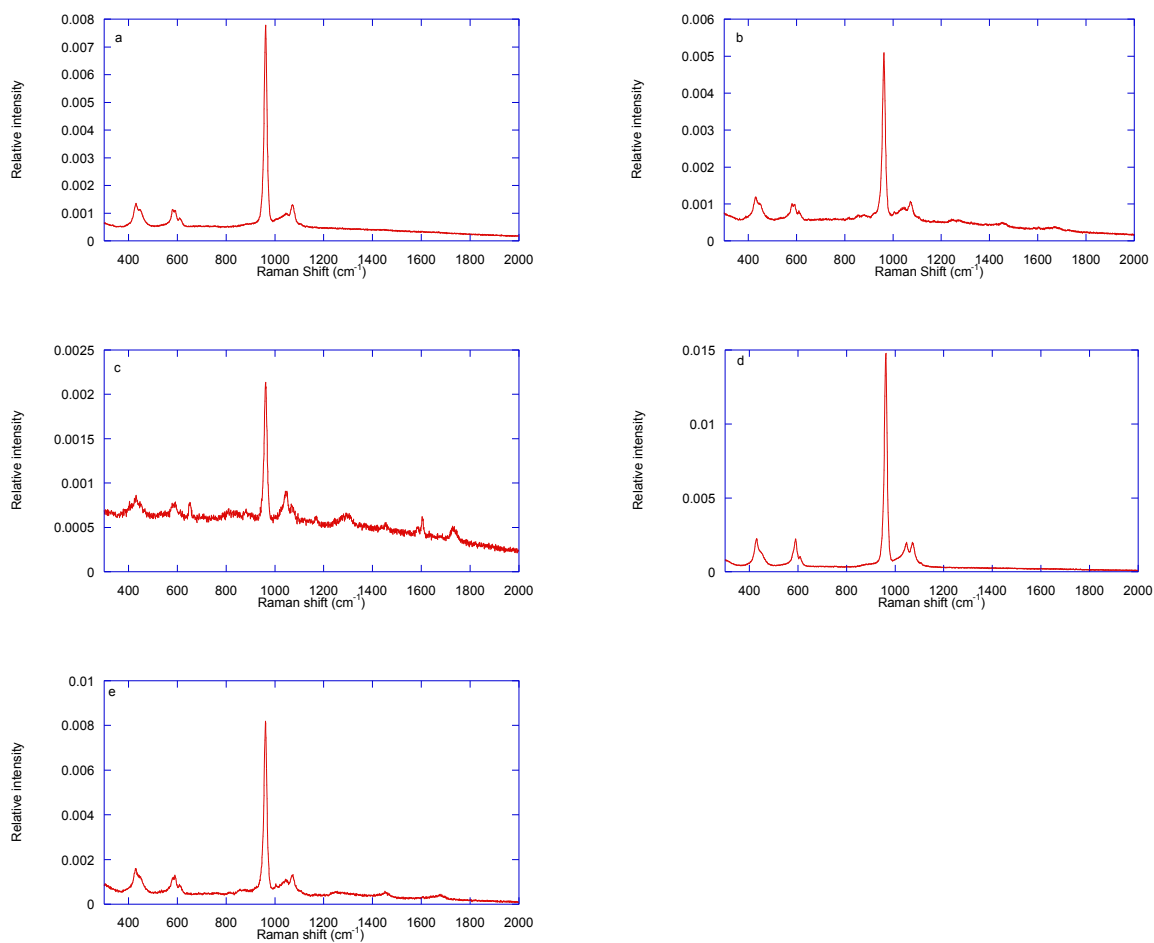
Figure 3.2.2. Raman spectra from the human teeth samples in the area of the enamel (**a, d**), dentin (**b, e**) and the Dental enamel junction (**c**) for the Adult tooth (**a-b**) and deciduous tooth (**d,e**). All spectra are dominated by the v1 phosphate peak, the dentin samples show a slight organic component in the 1400-1700 cm^{-1} range, which were not detected in the enamel.
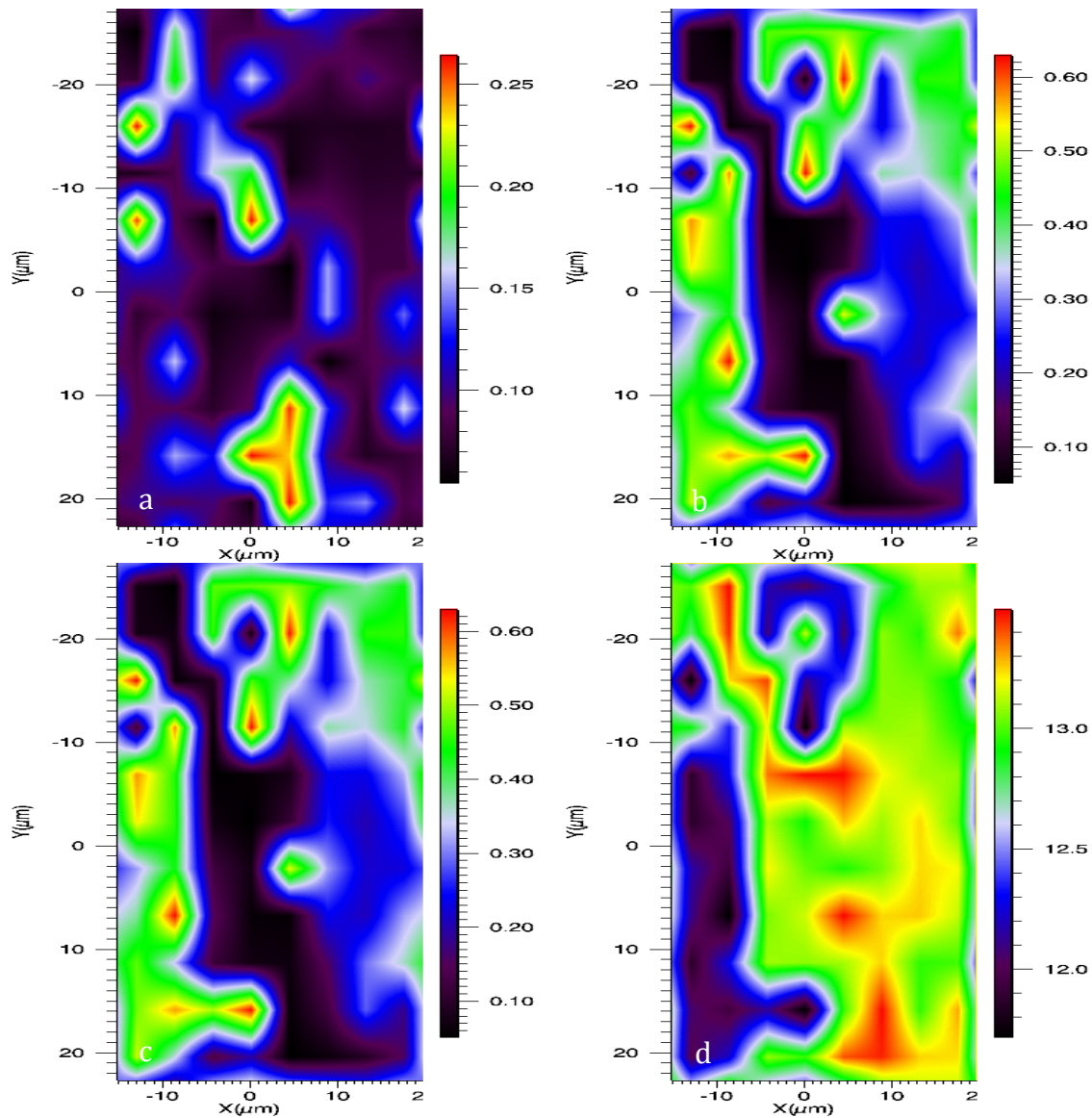
Figure 3.2.3. Raman mapping data from the adult tooth showing the (**a**) carbonate to phosphate ratio, (**b**) amorphous phosphate to crystalline phosphate ratio, (**c**) v1 phosphate position and (**d**) v1 phosphate width.
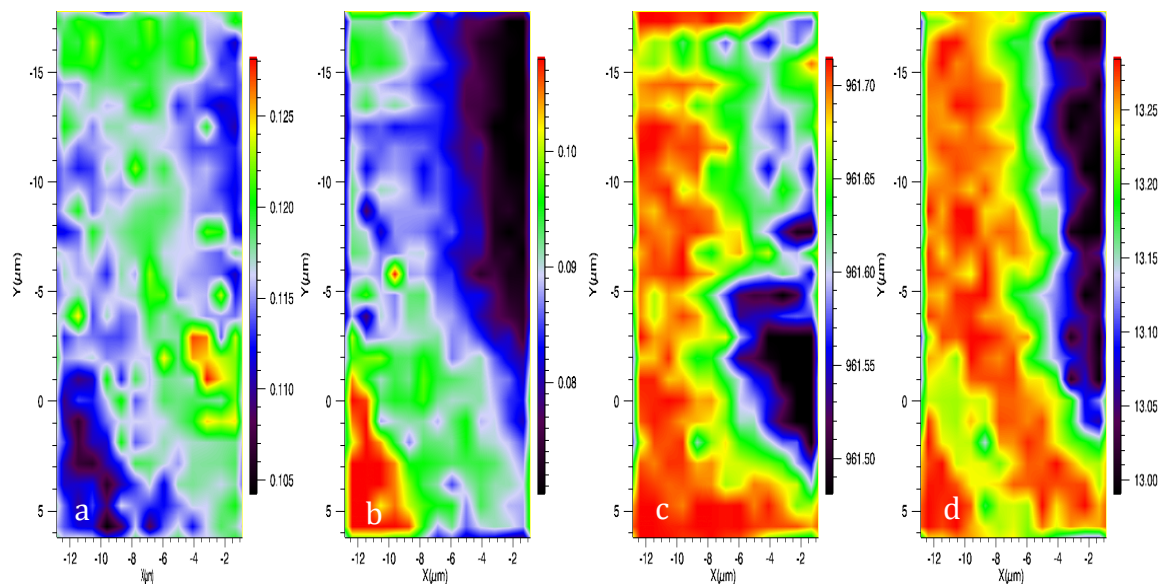
Figure 3.2.4. Raman mapping data from the deciduous tooth showing the (**a**) carbonate to phosphate, (**b**) amorphous phosphate to crystalline phosphate, (**c**) v1 phosphate position and (**d**) v1 phosphate width.
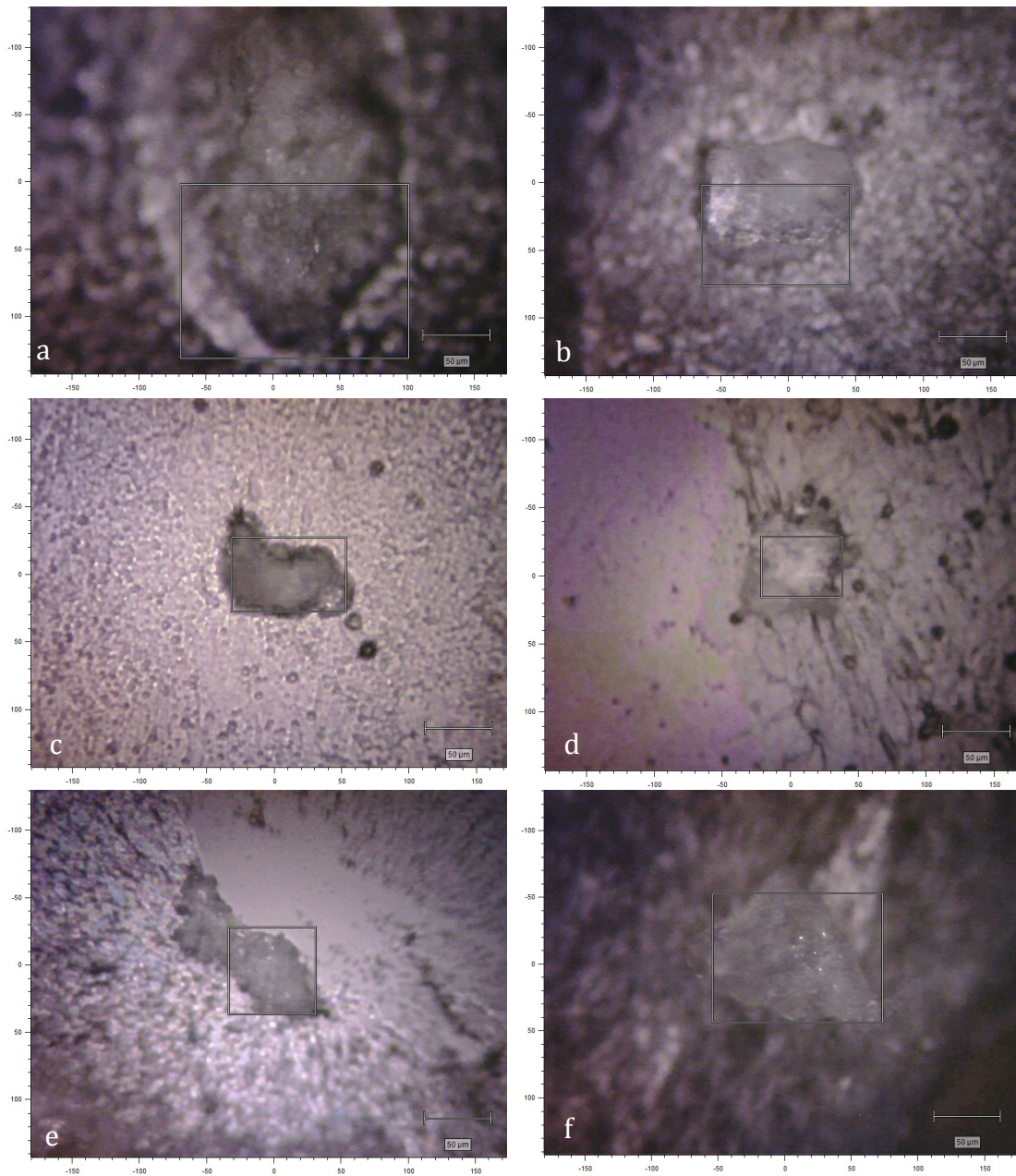
Figure 3.3.1. White light images of mineralized nodules from the dentin stem cells, at 50x magnification. The areas in the box are the regions over which the Raman mapped. Mineralized nodules where found in the (**a**) BCMP, (**b**) DPA, (**c**) GF, (**d**) PDL, (**e**) SCAP and (**f**) SHED cell lines.
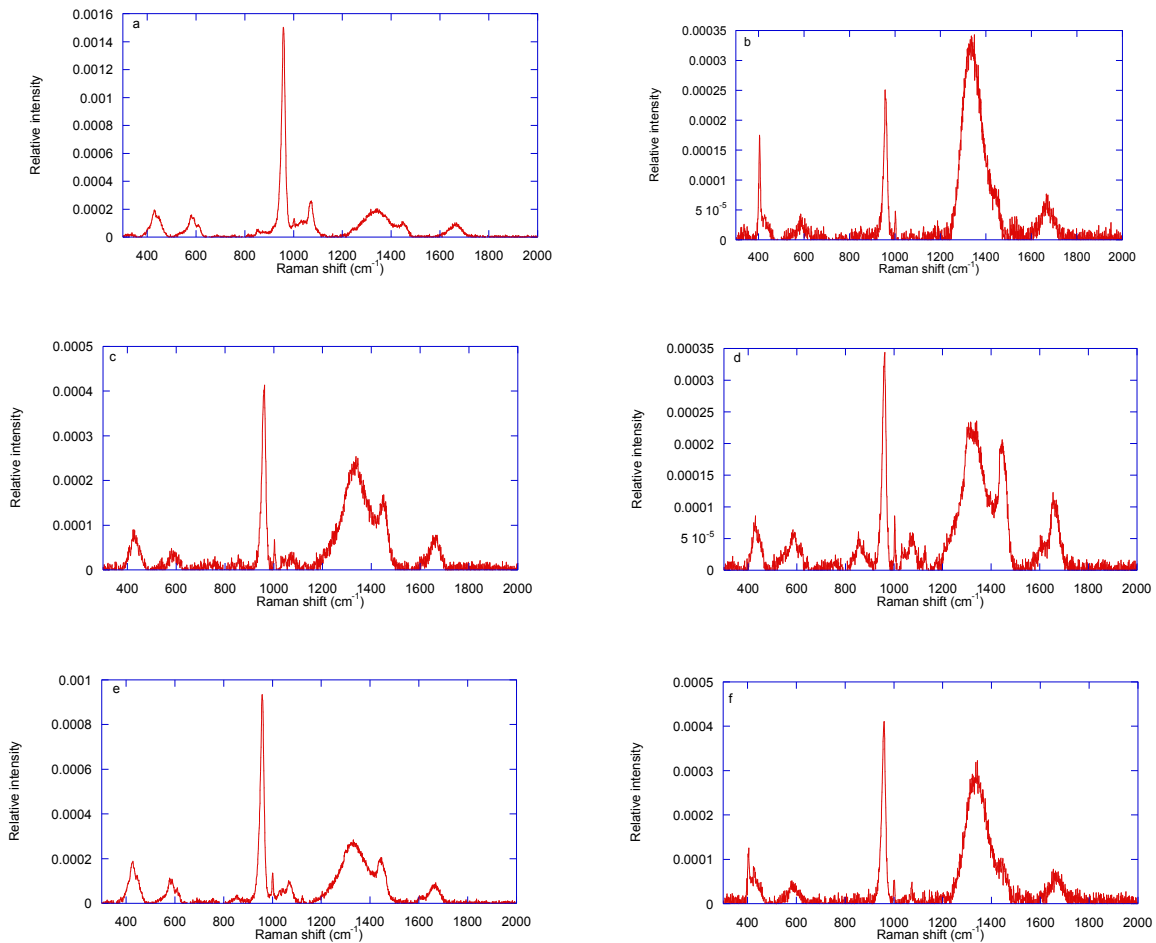
Figure 3.3.2. Raman spectra from mineralized nodules of dentin stem cells of (**a**) BCMP, (**b**) DPA, (**c**) GF, (**d**) PDL, (**e**) SCAP and (**f**) SHED cell lines. As well as a spectra of the magnesium fluoride substrate (**g**). All of the mineralized nodules exhibited features of hydroxyapatite, with the v1 phosphate peak at 960 cm^{-1}. The dental stem cell lines all formed mineralized nodules. Large absorptions from the magnesium fluoride substrate were present in all samples.
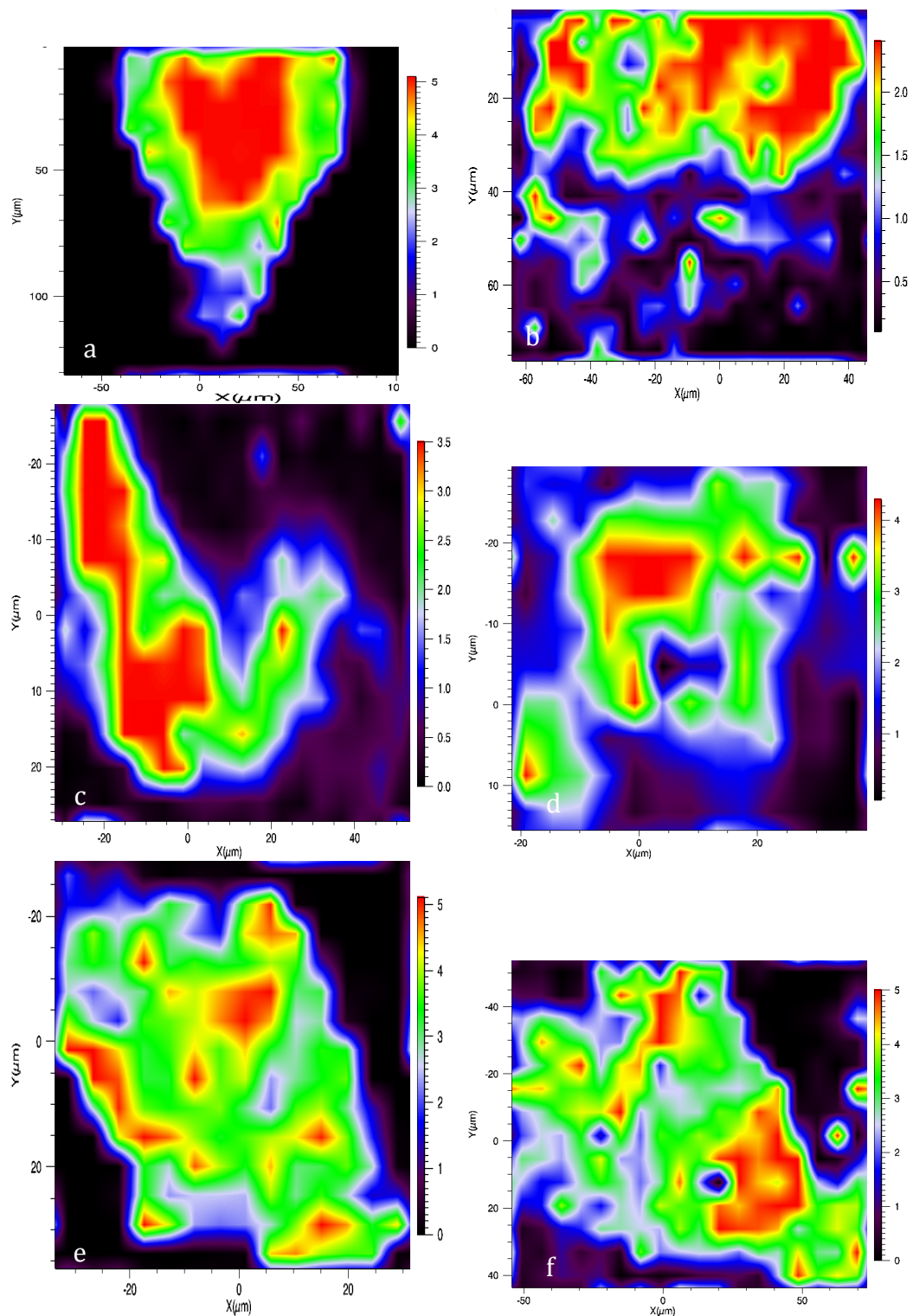
Figure 3.3.3. Mineral to matrix ratio calculated by the area under the v1 phosphate peak divided by the area of the amide I peak, for the (**a**) BCMP, (**b**) DPA, (**c**) GF, (**d**) PDL, (**e**) SCAP and (**f**) SHED cell lines.
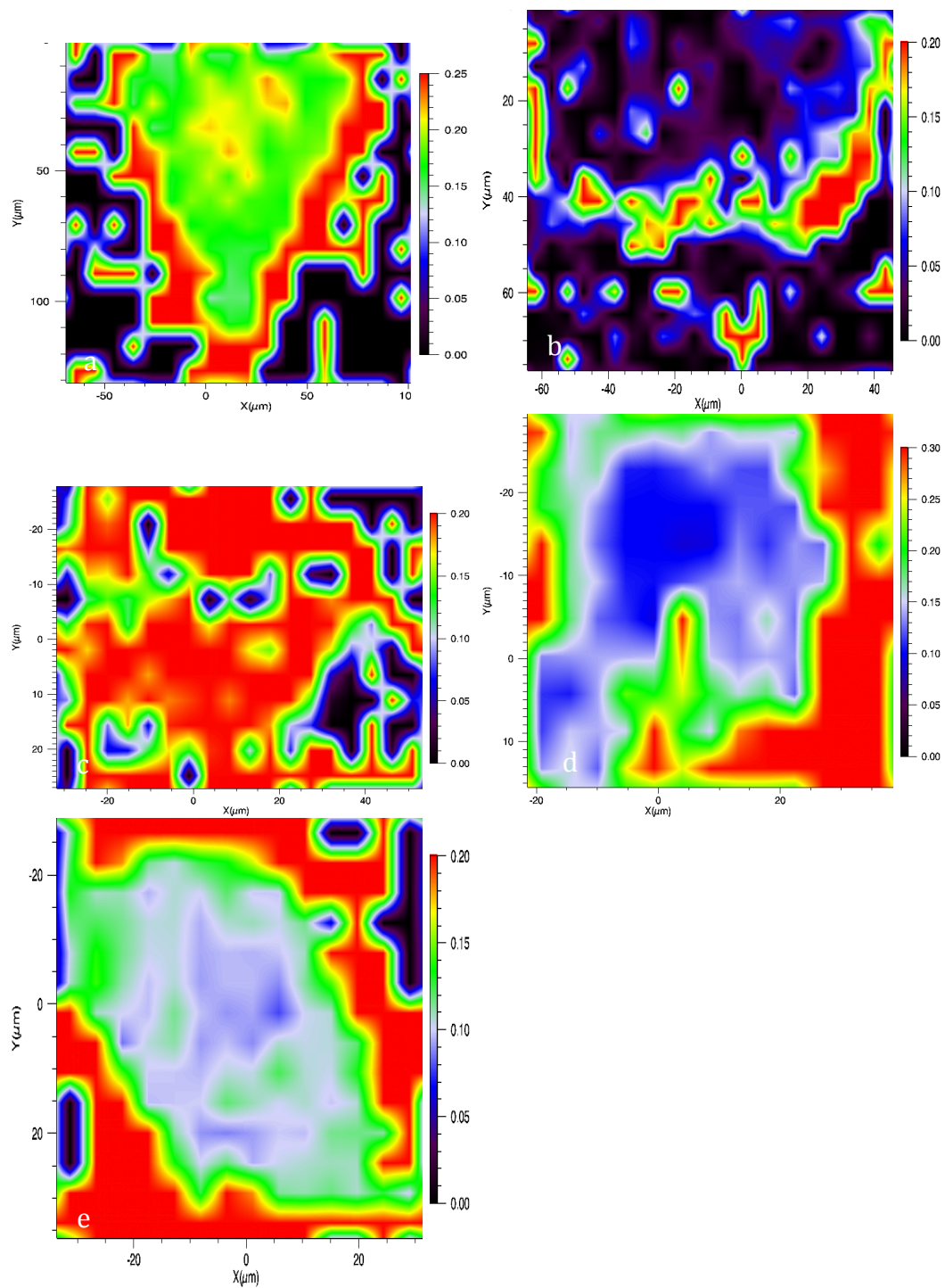
Figure 3.3.4 Carbonate to phosphate ratio calculated by the area under the 1070 cm^{-1} carbonate peak divided by the area of the v1 phosphate peak. For (**a**) the BCMP, (**b**) DPA, (**c**) GF, (**d**) PDL and (**e**) SCAP cell lines.   The carbonate to phosphate ratio for the SHED sample could not be accurately determined.
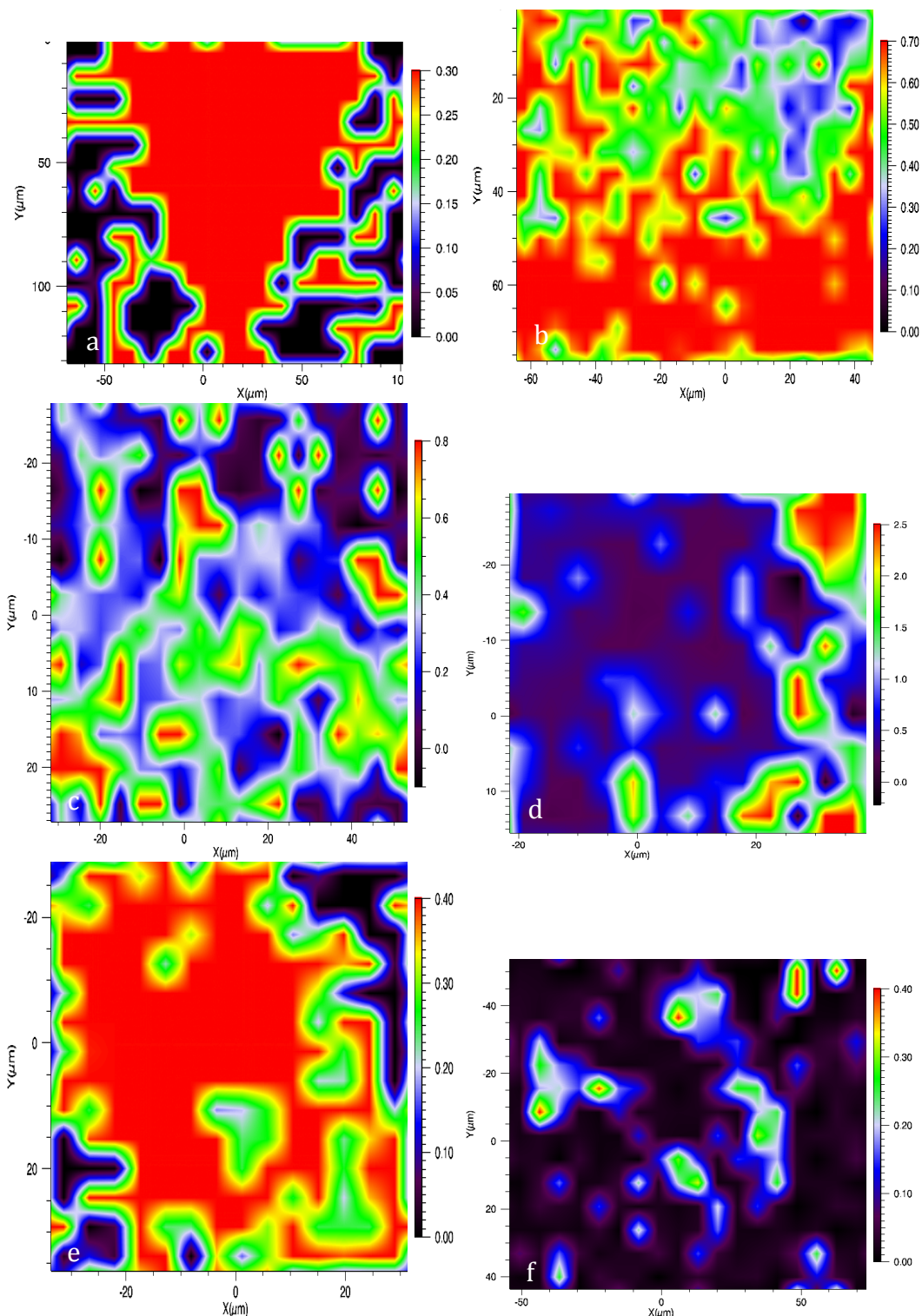
Figure 3.3.5. Amorphous Phosphate to Crystalline Phosphate phosphate ratio calculated by the area under the 950 cm^{-1} amorphous phosphate peak divided by the area of the v1 phosphate peak. For the (**a**) BCMP, (**b**) DPA, (**c**) GF, (**d**) PDL and (**e**) SCAP cell lines.
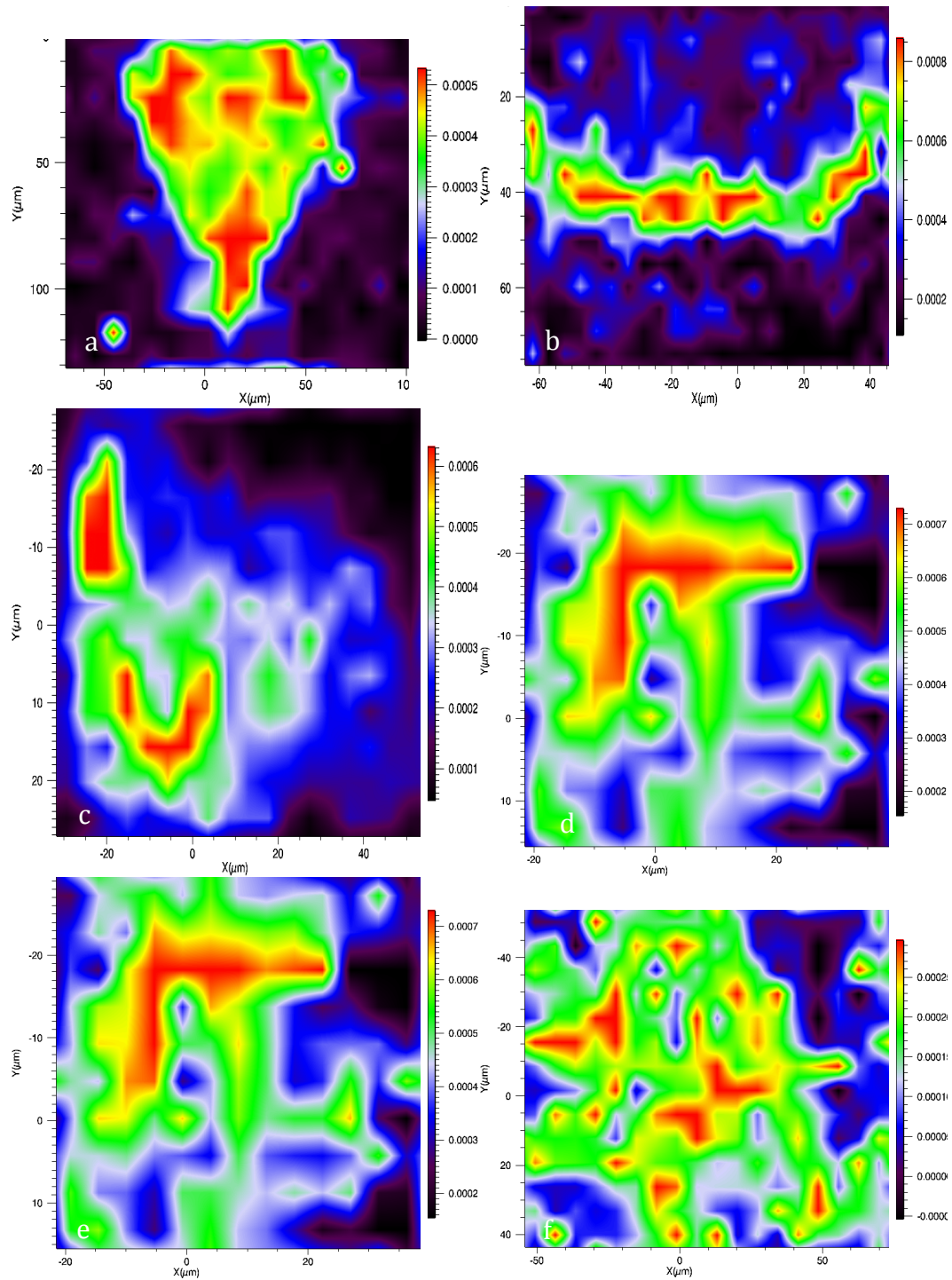
Figure 3.3.6. The area under the collagen curve plotted as a function of position. For the (**a**) BCMP, (**b**) DPA, (**c**) GF, (**d**) PDL and (**e**) SCAP cell lines.
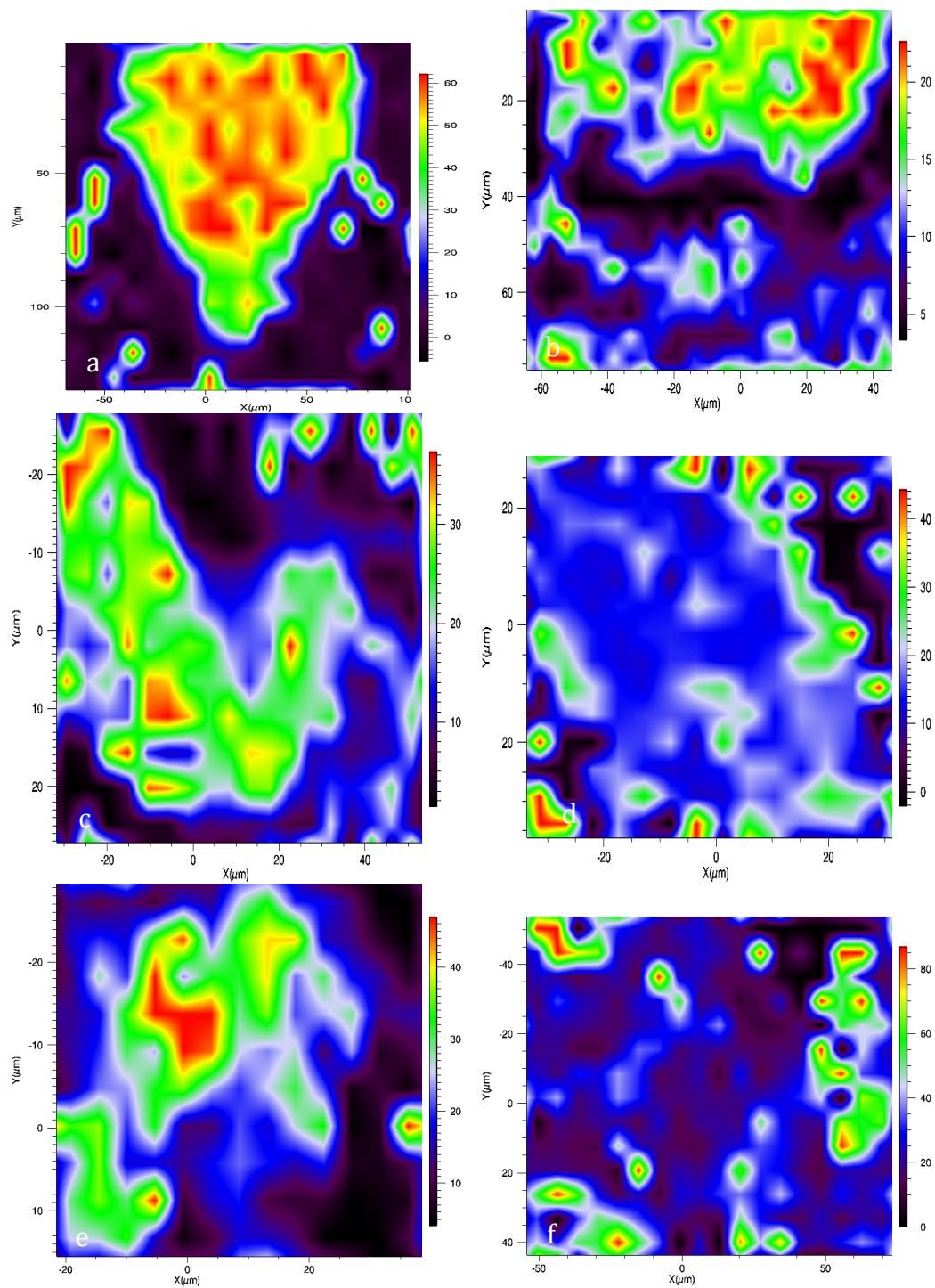
Figure 3.3.7. Raman mapping data of the v1 phosphate (960 cm^{-1}) area to the collagen (1003 cm^{-1}) area for (**a**) the BCMP, (**b**) DPA, (**c**) GF, (**d**) PDL, (**e**) SCAP and (f) SHED cell lines.
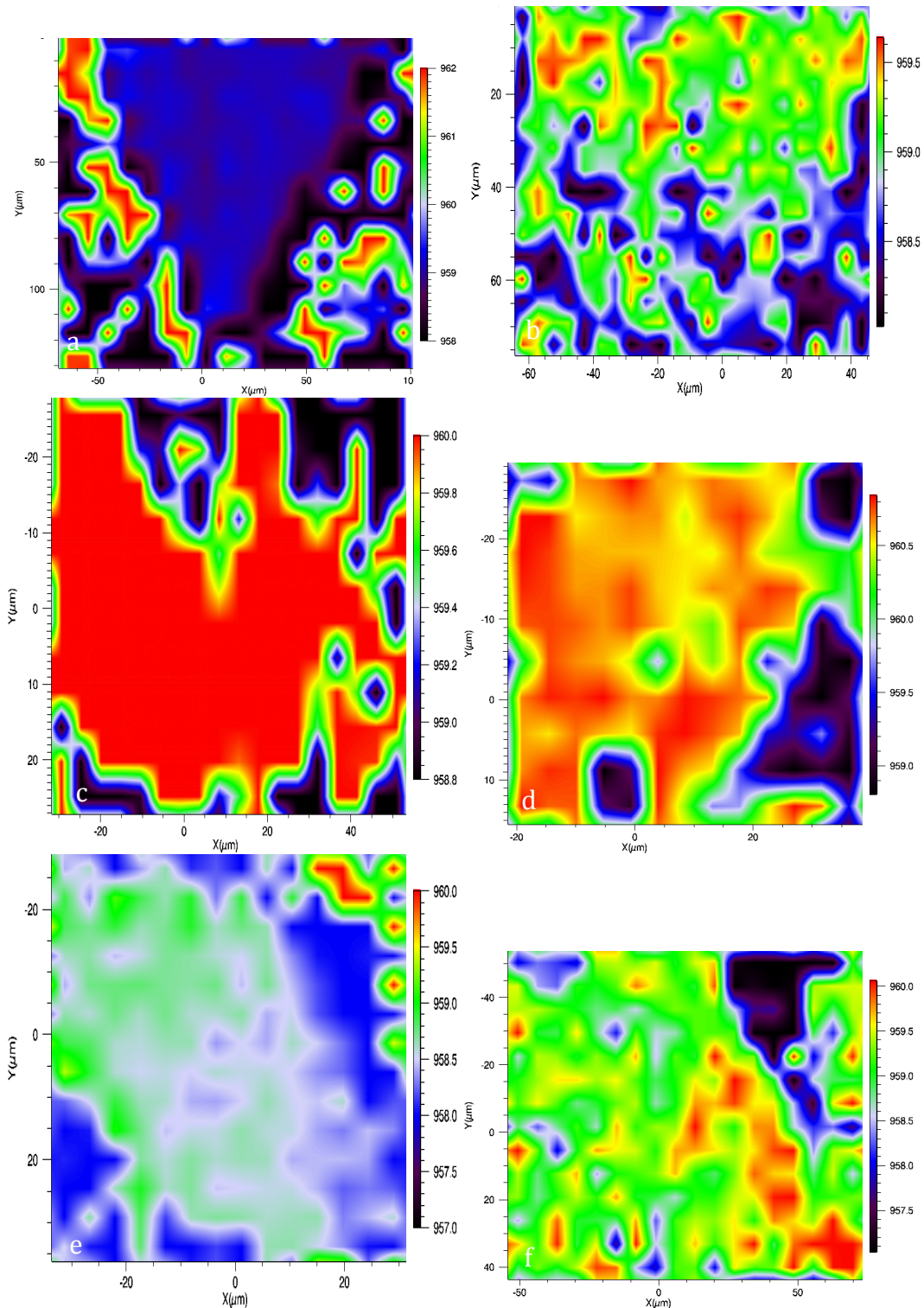
Figure 3.3.8. The peak position of the v1 phosphate peak plotted as a function of position. A shift of the peak position is indicative of a change in stress in the mineral component of the sample. Peak position of the v1 phosphate peak for the (**a**) BCMP, (**b**) DPA, (**c**) GF, (**d**) PDL and (**e**) SCAP cell lines.
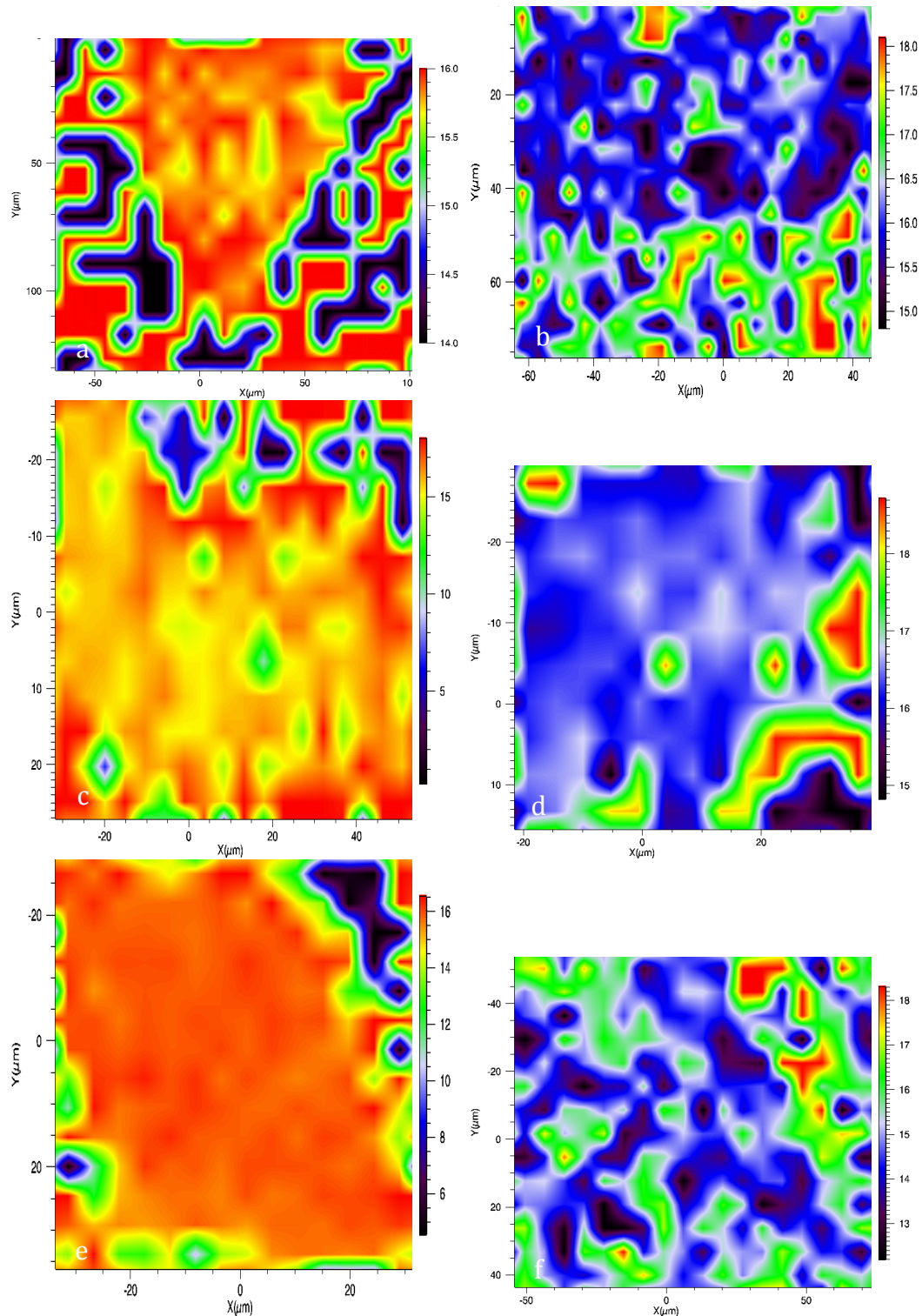
Figure 3.3.9. The full width at half max of the v1 phosphate peak plotted as a function of position. A change in the peak width is indicative of a change in crystallinity in the mineral component of the sample. Peak width of the v1 phosphate peak for the (**a**) BCMP, (**b**) DPA, (**c**) GF, (**d**) PDL and (**e**) SCAP cell lines are shown.
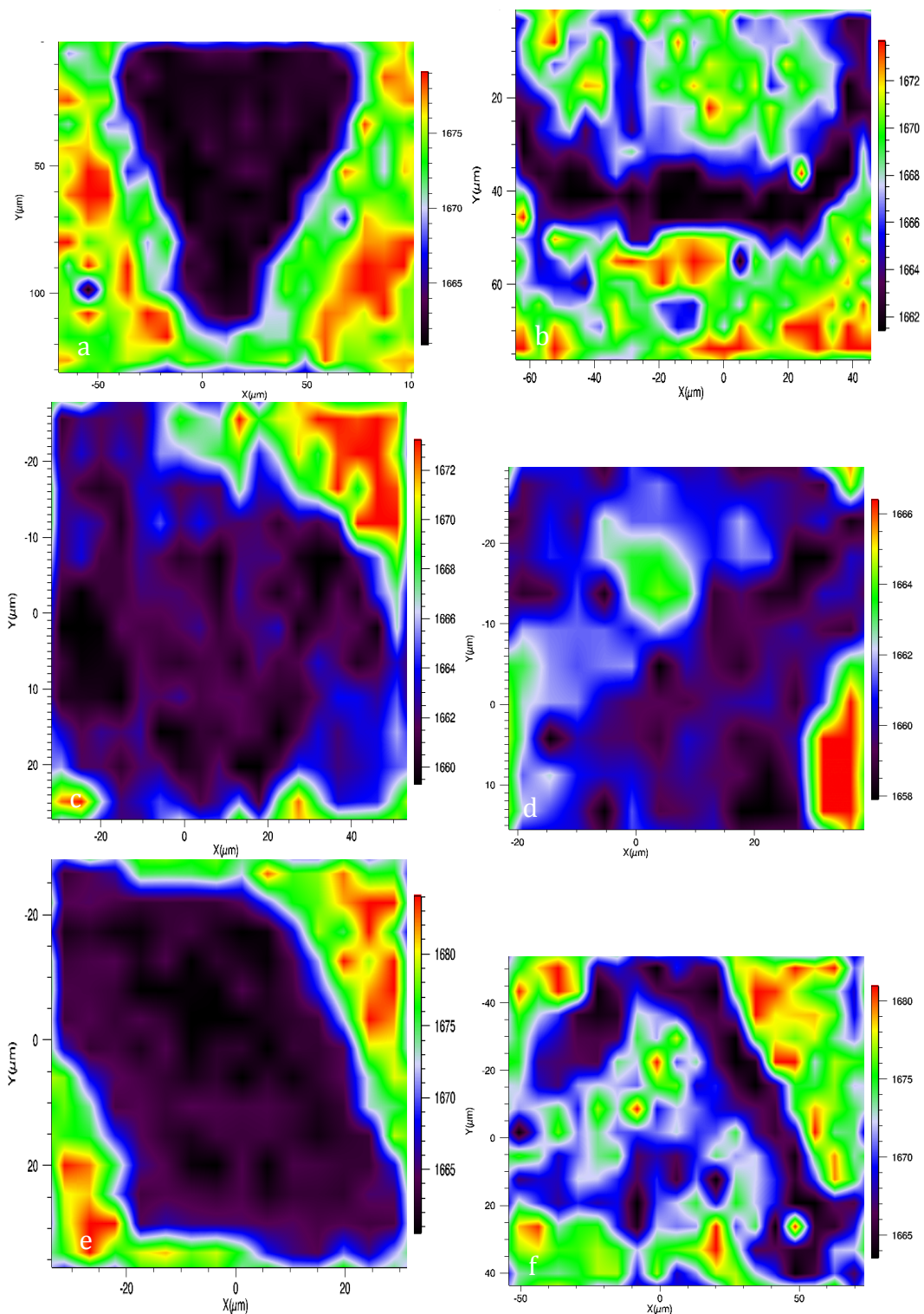
Figure 3.3.10. The peak position of the amide I peak plotted as a function of position. A shift of the peak position is indicative of a change in stress in the mineral component of the sample. Peak position of the amide I peak for the (**a**) BCMP, (**b**) DPA, (**c**) GF, (**d**) PDL and (**e**) SCAP cell lines.
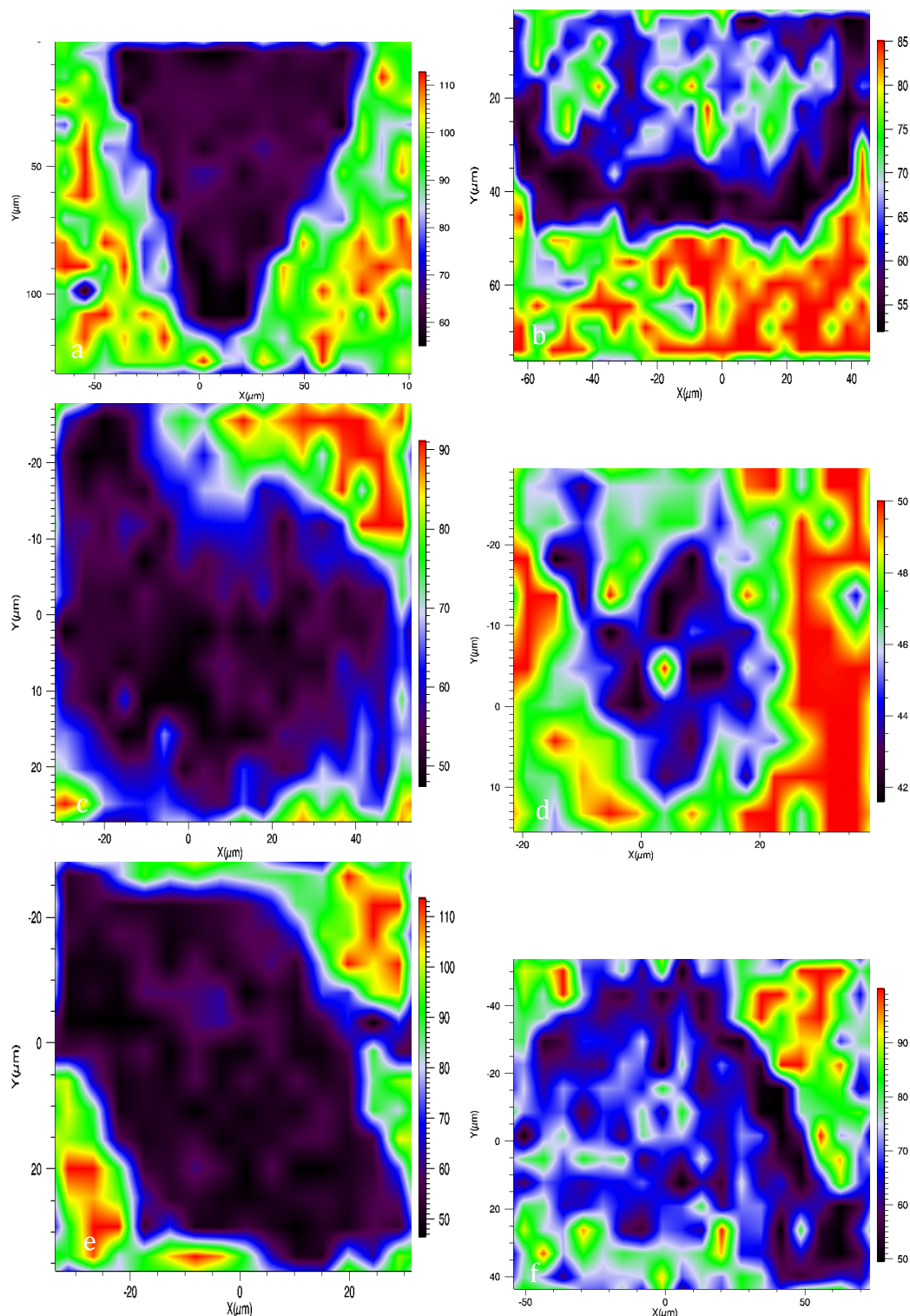
Figure 3.3.11. The full width at half max of the amide I peak plotted as a function of position. A change in the peak width is indicative of a change in crystallinity in the mineral component of the sample. Peak width of the amide I for the (**a**) BCMP, (**b**) DPA, (**c**) GF, (**d**) PDL and (**e**) SCAP cell lines are shown.
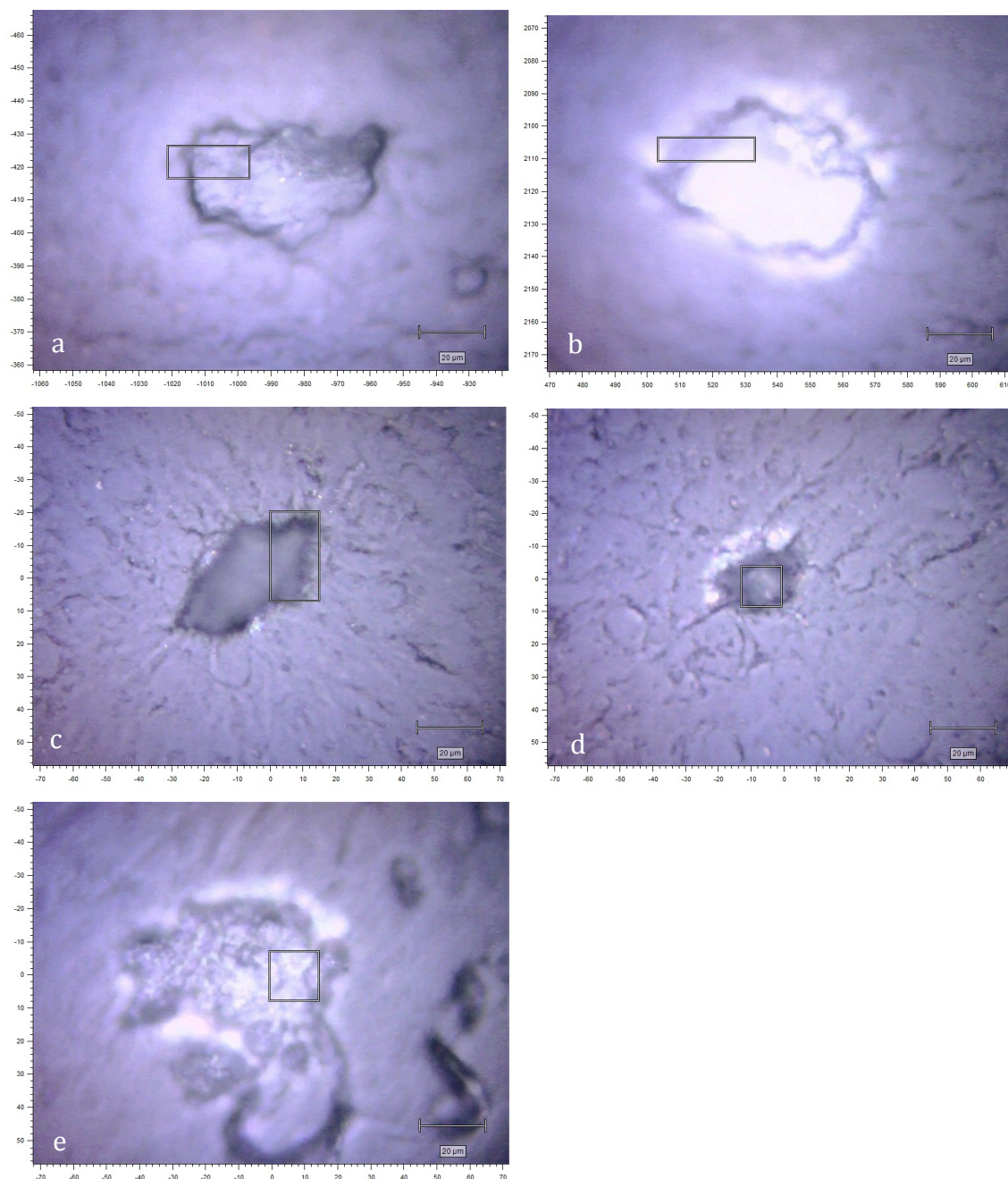
Figure 3.5.1. White light images the formation of nodules from osteoblasts on titania substrates, at 50x magnification. The areas in the box are the regions over which the Raman mapped. No mineralization was detected in any of these samples, the deposits were determined to be collagen and other organic compounds essential to the mineralization process. Five different titiana substrates were tested, four heat-treated at (b) 200 *C, (**c**) 300 *C, (d) 400 *C and (**e**) 600 *C, as well as one (**a**) as received sample.

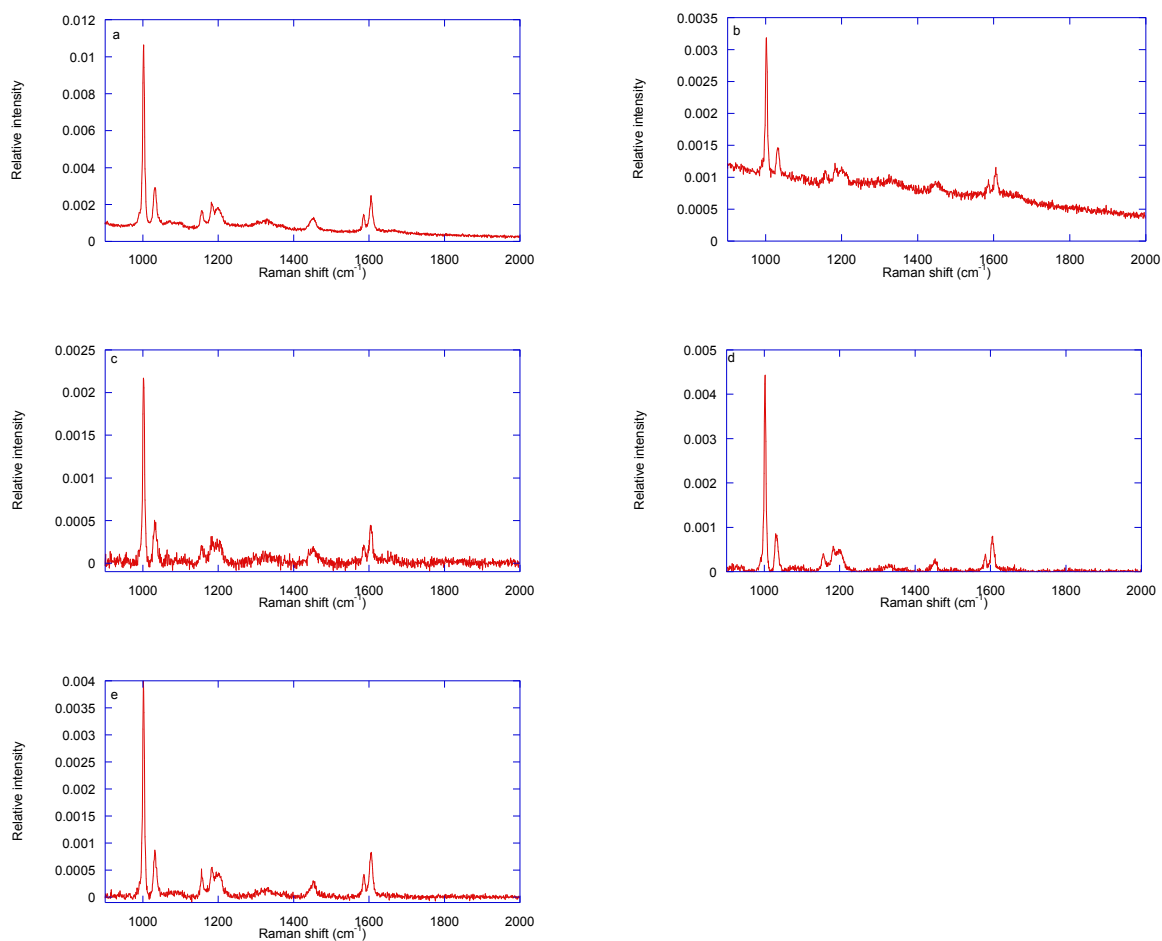**Figure 3.5.2.** Raman spectra of osteoblasts cultured for 14 days on titania substrates. Titania substrates where heat treated at (**b**) 200 °C, (**c**) 300 °C, (**d**) 400 °C and (**e**) 600 °C, as well as one (**a**) as received sample.

Table 3.3						
Sample	Mineral to matrix Ratio	Carbonate to Phosphate Ratio	Phosphate width (cm^{-1})	Phosphate Position (cm^{-1})	Amide I Width (cm^{-1})	Amide I position (cm^{-1})
BCMP	5.0	0.19	15.97	959.0	75	1667
DPA	2.3	0.20	17.28	958.4	80	1665
GF	3.5	0.15	15.91	960.6	65	1660
PDL	4.2	0.17	15.93	960.3	50	1659
SCAP	3.9	0.13	15.91	958.6	56	1670
SHED	5.2	n/a	17.45	958.4	68	1680

Table 3.3. Table detailing the data from the dental stem cell nodules.

Table 3.4							
Sample Number	1	2	3	4	5	6	7
960 Shoulder /960 Ratio	0.176±0.012	0.166±0.011	0.174±0.013	0.226±0.012	0.19±0.008	0.182±0.014	0.184±0.012
Peak Position	963.455±0.003	962.931±0.006	963.892±0.011	962.931±0.001	964.025±0.014	963.323±0.002	964.059±0.046
Peak Width	07.006±0.006	06.984±0.016	06.009±0.026	07.452±0.004	07.131±0.015	08.162±0.002	05.982±0.047

Table 3.4. Table detailing the phosphate peak from the peak analysis of the 960 cm^{-1} peak in the Raman spectra. The peak width and position is reported as well as the ratio of amorphous phosphate to crystalline phosphate in the coatings

Table 3.5					
	Collagen to nucleic acids	Collagen to protein	Nucleic Acid to protein	position	width
Heat-Treatment	1202 cm^{-1}/1382 cm^{-1}	1002 cm^{-1}/1157cm^{-1}	1328 cm^{-1}/1157 cm^{-1}	1003 cm^{-1}	1003 cm^{-1}
AR	5.13±0.53	9.52±1.07	2.26±0.97	1002.13±0.05	5.75±0.13
200	4.93±0.27	8.74±0.58	1.84±0.36	1002.56±0.06	5.67±0.12
300	5.36±0.64	8.72±0.42	1.89±0.93	1002.16±0.14	5.81±0.6
400	6.05±0.55	8.96±0.7	1.61±0.4	1002.14±0.08	5.65±0.13
600	4.48±0.7	10.46±0.98	2.99±1.22	1002.13±0.07	5.69±0.26

Table 3.5. Table detailing the collagen peak properties from the peak analysis of the Raman spectra. The ratio of the characteristic 1002 cm^{-1} collagen peak's to the nucleic acid signals a 1382 cm^{-1} and protein absorptions at 1157 cm^{-1} are reported along with the position and width of the 1002 cm^{-1} peak.